# Mobility &
# Vehicle
# Mechanics

*International Journal for Vehicle Mechanics, Engines and Transportation Systems*

# M V M  Mobility Vehicle Mechanics

*Editors: Prof. dr **Jovanka Lukić**; Prof. dr **Čedomir Duboka***

**MVM** *Editorial Board*
*University of Kragujevac*
*Faculty of Engineering*
*Sestre Janjić 6, 34000 Kragujevac, Serbia*
*Tel.: +381/34/335990; Fax: + 381/34/333192*

# Mobility &

# Motorna

# Vehicle

# Vozila i

# Mechanics

# Motori

# Mobility &     Motorna

## Vehicle

Vozila i

## Mechanics     Motori

# DESIGN METHOD FOR HYDRODYNAMIC TORQUE CONVERTER

*Dobrica Milovanović [1*], Dušan Gordić [2], Vladimir Vukašinović [3], Mladen Josijević [4]*

RESEARCH ARTICLE

**ABSTRACT:** The design of hydrodynamic torque converter impeller is a complex problem that can be solved if the whole set of individual steps is carried out, starting from input data selection to determination of the model sections of the blade. For that reason, fast as well as efficient solution of inverse flow problem can be carried out only by using numerical techniques to solve fluid flow problems. The method developed in this paper, based on free vortex design, involves the linking of meridional and blade-to-blade solutions. A basic assumption used for predicting flow in the meridional plane of the hydrodynamic transmissions impeller is an axisymmetric flow. In accordance with the Bauersfeld method, the design of the impeller blade is performed in an iterative manner using the relationships between velocity components and geometrical blade parameters. Particular attention in the paper is paid to the determination of a functional law of the energy interchange from the inlet to the outlet in the pump and turbine impeller in hydrodynamic transmissions. Finally, a design example for the pump impeller blade is presented.

**KEY WORDS**: torque converter, axisymmetric flow, energy interchange, design, blade

[1]*Dobrica Milovanović, PhD, full prof., University of Kragujevac, Faculty of Engineering, Sestre Janjić 6, 34000 Kragujevac, Serbia, dobrica@kg.ac.rs (\*Corresponding author)*
[2]*Dušan Gordić, PhD, full prof., University of Kragujevac, Faculty of Engineering, Sestre Janjić 6, 34000 Kragujevac, Serbia, gordic@kg.ac.rs*
[3]*Vladimir Vukašinović, PhD, assist. prof., University of Kragujevac, Faculty of Engineering, Sestre Janjić 6, 34000 Kragujevac, Serbia, vladimir.vukasinovic@kg.ac.rs*
[4]*Mladen Josijević, Assistant, University of Kragujevac, Faculty of Engineering, Sestre Janjić 6, 34000 Kragujevac, Serbia, mladen.josijevic@fink.rs*

# METOD PROJEKTOVANJA HIDRODINAMIČKIH TRANSMISIJA

**REZIME**: Projektovanje radnih kola hidrodinamičkih transmisija predstavlja kompleksan problem koji se može uspešno rešiti samo ukoliko se čitav niz pojedinačnih koraka pravilno izvrše, počev od izbora ulaznih podataka pa do definisanja modelskih preseka lopatica. Iz tog razloga, brzo i efikasno rešavanje, tzv. inverznog strujnog zadatka moguće je jedino korišćenjem numeričke simulacije strujanja fluida. Metod, predložen u ovom radu, podrazumeva povezivanje rešenja strujanja u meridijanskoj i cirkularnoj ravni. Osnovna pretpostavka, korišćena pri rešavanju postavljenog zadatka odnosi se na osnosimetričnost strujnog polja. U skladu sa metodom Bauersfelda, projektovanja lopatica radnog kola izvršeno je u iterativnom postupku uz korišćenje relacija koje povezuju brzinsko polje sa geometrijskim parametrima lopatice. Posebna pažnja u radu je posvećena definisanju funkcionalne zavisnosti razmene enrgije od ulazno do izlazne ivice lopatice radnog kola. Na kraju rada prikazan je primer dizajniranja lopatica pumpnog kola.

**KLJUČNE REČI**: hidraulična transmisija, osnosimetrično strujanje, razmena energije, projektovanje, lopatica

# DESIGN METHOD FOR HYDRODYNAMIC TORQUE CONVERTER

*Dobrica Milovanović, Dušan Gordić, Vladimir Vukašinović, Mladen Josijević*

## 1.    INTRODUCTION

A hydrodynamic torque converter is a type of fluid coupling which transmits power from the engine shaft to the transmission shaft. It is a crucial component in the drivetrain of a vehicle equipped with an automatic gearbox. A typical torque converter consists of the three major components: pump, turbine, and stator (Figure 1). A pump is attached to the engine shaft (prime mover) while the turbine is connected to the transmission shaft. The stator, which is placed between the pump and the turbine, redirects the returning fluid from the turbine to the pump. A one-way clutch is used along with the stator to either lock or unlock the stator depending on the fluid direction (whether it hits the front or back of the stator's vanes). Thus, the pump is used to energize the working fluid which then drives a turbine and returns the fluid to the pump through the stator in a closed circuit [1]. As its name implies, the stator is normally stationary but in most modern torque converters it is usually fitted with a one-way clutch. The torque converter plays an important role in transmitting the engine's torque during the multiplication (converter) and coupling (lock-up) modes. It greatly improves vehicle launch characteristics and passenger comfort [2], thus improving the overall drive ability of the vehicle.
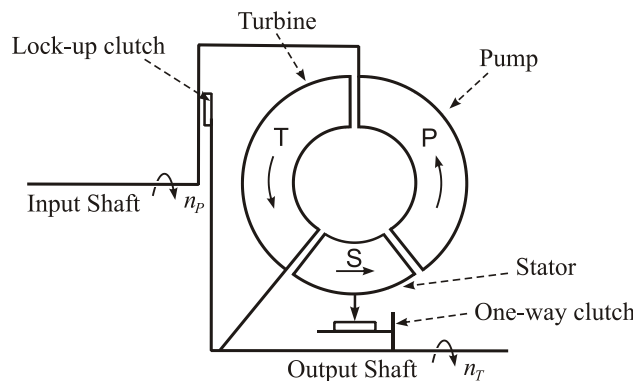


**Figure 1**. Cross section of a torque converter

## 2.    BACKGROUND

A mathematical formulation of the flow field (a direct problem of turbomachinery) inside a torque converter has been developed and published by number of authors, among the others by Kotwicki [3], Hrovat and Tobler [4] and Ejiri and Kubo [5]. The calculation models of the hydrodynamic torque converter have been widely discussed by Migus et al. [6].

The design of the pump (Figure 2) and turbine impeller blades, in general, is the problem of solving the inverse stream task. This problem means obtaining the blade shape on the basis of an already defined stream field, in relation to the given characteristic of the turbomachinery [7]. Concerning the inverse design of turbomachinery blades many papers were published in past years [8]. For the difficulty of inverse problem these models were developed basically under assumption of inviscid flow considering that the effect of fluid viscosity mainly dominates in a thin layer near to solid boundaries in actual machines [9].

Based on Wu's theory of two-type stream surfaces [10], quasi three-dimensional (Q3D) inverse models were developed by iterative calculation of a mean hub-to-tip (*S2m*) stream surface and a series of blade-to-blade (*S1*) stream surfaces [11]. Q3D inverse methods based on *S1* surface or *S2m* surface were extended to various type of turbomachinery [12]. Chen et al. [13] and Borges [14] presented a method for solving the inverse (design) problem of blade cascade flow on the blade-to-blade stream surface of revolution on the basis of the fundamental equations of fluid dynamics.
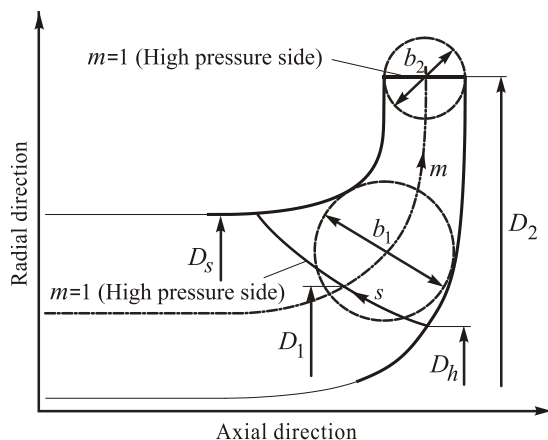
**Figure 2**. Sketch of pump impeller meridional plane (*S2m*)

Because of the complexity of stream phenomena in turbomachinery, the solution of a three-dimensional flow equation presents a formidable problem. In general, the flow is unsteady, viscous and compressible and subjected to complicated boundary conditions [15]. Even assuming that the flow is steady and inviscid, the problem still remains very difficult.

In order to obtain the solution of the inverse problem in hydraulic turbomachinery Barlit [16] proposed some assumption that should simplify the problem.

The first assumption is neglecting the viscous characteristic of a working fluid, which enables the use of the theory of the inviscid and incompressible fluid. Figure 3 shows a justification of this assumption. According to Kanavagh [17] the velocity profiles for potential flow and turbulent flow coincide well (Fig. 3).
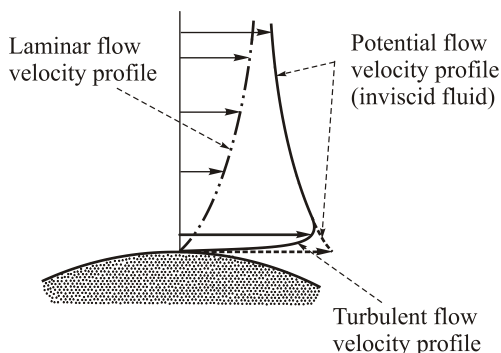
**Figure 3.** Flow velocity profiles showing influence of the boundary over a range of Reynolds number from laminar to potential flow

The second assumption presents neglecting the unsteadiness of the flow that is caused by the finite number of impeller blades. The third assumption in solving the inverse problem in turbomachinery is the simplification of real three-dimensional flow to the quasi-two-dimensional flows. This is achieved by taking the mean value of the flow equations with respect to tangential coordinate. This way, the flow in the impeller can be considered as a sum of two components of quasi-two-dimensional flow, as follows:

1. flow in the meridional plane
2. flow in blade-to-blade surfaces

More advanced, three dimensional approaches for the solution of an inverse problem are presented by Chen et al. [18] and Yang et al. [19].

## 3. THE FLOW PROBLEM FORMULATION

The flow in blade-to-blade surfaces can be considered as two-dimensional only for solution of the direct flow problem. In the case of the inverse flow problem that approach increases a problem complexity. For that reason, in this paper, instead of two-dimensional flow, one-dimensional flow is considered. In order to correct this assumption in the calculation procedure the corresponding coefficients, which take into account the difference between the simplified flow model and real flow, are introduced.

In accordance with the usual methodology for inverse problem solution with the assumption mentioned, design procedure can be divided into two phases:

1. Solution of the meridional flow in order to define the axially symmetric flow surfaces.
2. Definition of the basic geometric characteristics of the cascades of space profile on the axially symmetric flow areas defined in the previous step.

In this paper, the mathematical model for inverse problem solution is based on the Bauersfeld method [20], which is commonly used in the design of mixed flow type impellers. The Bauersfeld method considers potential meridional flow ($\Omega_u = 0$) and during the procedure, impeller blades are considered as infinitely thin vortex areas (Figure 4).



**Figure 4.** Vortex line and corresponding blade for $\Omega_u = 0$

In the case of the potential meridional flow vortex vector

$$\Omega = \Omega_m = \Omega_r + \Omega_z$$

lies in the meridional plane and from the vortex line equation [20] in the meridional plane:

$$\Omega_r dz - \Omega_z dr = 0 \tag{1}$$

after the introduction of the vortex components,

$$\Omega_r = \frac{\partial(rc_u)}{r\partial z} \quad \text{and} \quad \Omega_r = -\frac{\partial(rc_u)}{r\partial r} \tag{2}$$

follows

$$\frac{\partial(rc_u)}{r\partial z}dz + \frac{\partial(rc_u)}{r\partial r}dr = 0 \tag{3}$$

or

$$rc_u = const. \tag{4}$$

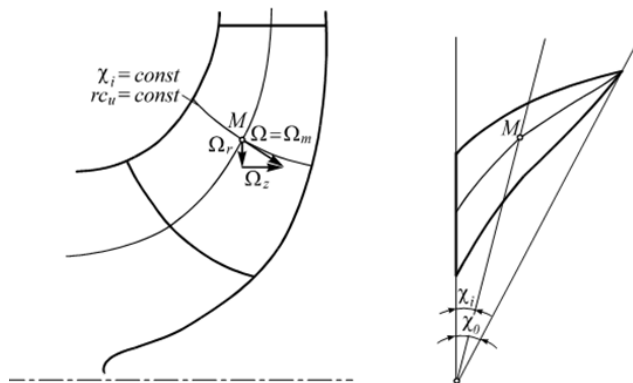From equation (4) it follows that the vortex value $rc_u$ along the vortex line is constant. Because the vortex line lies in the meridional plane and belongs to the blade, it will coincide with the section line of the blade and the corresponding meridional plane (radial blade section), $\chi_i = const.$ Thus, the vortex value $rc_u$ in the impeller is changed only from one radial section to another, which can be expressed as:

$$rc_u = f(\chi) \tag{5}$$

Outside the impeller, in the potential flow case, the vortex value is constant. According to the equations (4) and (5) that is possible only if the inlet and outlet edge of the blade lies in the meridional planes.

The design of the impeller blades is performed using relations between velocity components and geometrical blade parameters. Taking into account the conditions for the Bauersfeld method ($\Omega_u = 0$, $rc_u = const.$ along the radial blade sections), this equation takes the relatively simple form [20]:

$$d\chi = \frac{rc_u - r^2\omega}{r^2 c_m}ds \tag{6}$$

## 4.  DESIGN OF THE IMPELLER BLADES

### *4.1 Determination of the meridional flow*

The choice of the meridional flow type and method for its forming is the first step for the determination of the meridional flow. In this case adoption of the Bauersfeld method for inverse procedure solution means the adoption of the potential meridional flow. It is known that potential flow in the meridional planes is described with the Stokes equation [21]:

$$\frac{\partial}{\partial r}\left(\frac{1}{r}\frac{\partial\Psi}{\partial r}\right) + \frac{\partial}{\partial z}\left(\frac{1}{r}\frac{\partial\Psi}{\partial z}\right) = 0 \tag{7}$$

Solution of this equation is obtained using the finite element method [22]. That gives the values of the stream function in nodal points. The accuracy of the results of the calculation is defined by fineness of the finite element mesh, i.e. by the number of "the partial impellers".

Further, the lines $\Psi = const.$ are defined using *spline* interpolation (Figure 5) and the values of the meridional velocities are calculated using the expressions,

$$c_r = \frac{\partial\Psi}{\partial z}, \qquad c_z = -\frac{\partial\Psi}{\partial r} \tag{8}$$
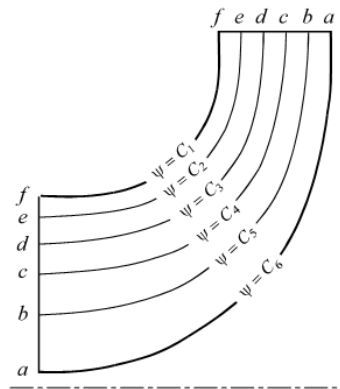
**Figure 5**. Streamline distribution for a potential meridional flow

### 4.2 Design of the impeller blades for potential meridional flow

For design of the impeller blade on the basis of equation (6), i.e. obtaining its radial sections, it is necessary to know the distribution of the tangential component of the absolute velocity $c_u$ along the meridional streamlines, (all other values are defined during the solution of the meridional flow). Because the value of the velocity $c_u$ is directly related to the energy balance between the fluid and impeller blades, it must be explicitly defined before the blade design itself. The whole procedure of the impeller blade design can be divided into two phases:

1. Definition of the functional law of the energy interchange in the impeller,
2. Definition of the blade shape which allows the defined law of the energy interchange.

#### 4.2.1 Determination of functional law of the energy interchange in the impeller

The calculation of this relation is performed based on the condition that in the impeller with an already defined blade angle $\chi_0$ in the circular plane the energy interchange has to be constant. Because the blade angle $\chi_0$ does not define the exact functional law of energy interchange, in general, there is some freedom in this procedure related to the curve type which define the mentioned law. On the other hand, on the basis of the present experience in the design of the impellers there some requirements which have to be taken into account if we want that the newly-designed impeller has good energy characteristics. Having this in mind, in order to achieve a good solution, in this paper the following conditions are imposed:

- along any meridional streamline the equal energy amount is interchanged
- the energy interchange between the fluid and the blades is continuous
- the biggest energy amount is interchanged near the outlet blade edge.

In accordance with the mentioned conditions, Figure 6 gives possible functional laws of energy interchange from inlet to the outlet of the impeller. The analytical expression which corresponds to the conditions mentioned above, and to the graph shown in Figure 6, can be described by the following analytical form [23]:

$$Y_{th} = Y_{th0}\left[1 - (1 - s/s_0)^{m\left(\frac{s}{s_0}\right)^k}\right] \tag{9}$$

where $k$ is the coefficient of curve type chosen at the beginning of the design procedure and $m$ is the coefficient formed during the procedure.
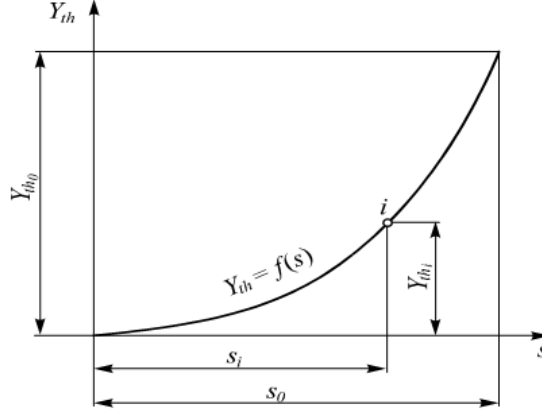


**Figure 6.** A convenient form of the energy interchange in the impeller

Determination of the energy interchange law, in this case, means determining the value of exponent $m$ in expression (9), based on the condition that along considered meridian streamline inside impeller energy interchange is $Y_{th0}$, for adopted blade angle $\chi_0$. The position of the meridional streamline inside the impeller and its length are defined by the prescription of the shape of the inlet and outlet edge of the blade in the meridional plane. A global solution of this problem is described below.

Adoption of the initial (free chosen) value of exponent $m$ presumes the exact law of the energy interchange and, on the basis of the Euler equation, the distribution of the tangential velocity component in the impeller. By dividing the meridional streamlines into $n$ equal parts $\Delta s$ (each can be considered as an elementary impeller), and finding corresponding angles $\Delta\chi_i$ (using equation (6)) and summing these, the total value of the angle $\chi$ in the circular plane can be calculated for proposed energy interchange law. This value is compared with angle $\chi_0$ and in the case that difference between them is greater than the prescribed value $\varepsilon\chi$ the iterative procedure is established until the convergence of exponent m is achieved.

In the mentioned procedure, from Euler equation for a finite number of blades,

$$Y_{th0} = u_2 c_{3u} - u_1 c_{0u} \tag{10}$$

and supposing zero inlet whirl ($c_{0u} = 0$), the value of the outlet velocity $c_{3u}$ is defined by

$$c_{3u} = \frac{Y_{th0}}{u_2} \tag{11}$$

The peripheral velocity $c_u$ inside impeller is determined from the actual energy interchange law (9), by the expression

$$c_{u\infty i} = \frac{Y_{thi}}{\omega r_i \varepsilon_i} \tag{12}$$

The coefficient $\varepsilon_i$ is calculated by Pfleiderer formula [24]:

$$\varepsilon_i = \frac{1}{1+(0.6\div1.0)(1+\beta_{Li}/60)\frac{r_i^2}{zS}} \qquad (13)$$

where static moment S of the meridional streamline inside impeller is calculated by

$$S = \int_{r_1}^{r_i} rds \qquad (14)$$

while blade angle $\beta_{Li}$ in the considered point follows from velocity triangle

$$\beta_{Li} = arctan\ \frac{c_{mi}}{u_i-c_{ui}} \qquad (15)$$

The meridional velocity for finite thickness is calculated using the expression,

$$c_{mi} = \frac{c_{mi\infty}}{1-\frac{z\delta_i}{2\pi r_i sin\beta_{Li}}} \qquad (16)$$

where $\delta_i$ is calculated from the corresponding blade thickness distribution along streamline inside the impeller

$$\delta_i = f(s) \qquad (17)$$

and length of the blade profile is given by

$$l_i = \sum_{k=1}^{i} \frac{\Delta s}{sin\beta_{Lk}} \qquad (18)$$

### 4.2.2 Determination of the blade shape

Under the condition defined by the Bauersfeld method, the vortex $rc_u$, i.e. stream energy in the impeller is changed only from one meridional plane to another. If the inlet edge of the blade lies in the meridional plane, the points on different meridional streamlines for equal energy interchange amount will lie on the meridional plane (another one) as well. Because of this, by connecting the ends of corresponding values $s_i$ on the different streamlines, the line that lies at the meridional plane is obtained. That line presents a section of the blade and the corresponding meridional plane (so-called radial section of the blade). If the number of radial sectiones is large enough, the corresponding blade shape is defined.



**Figure 7.** Radial section of the blade

The procedure of determination of the radial blade sections starts with a division of blade angle $\chi_0$ into *n* equal parts (Figure 7):

$$\Delta\chi = \frac{\chi_0}{n} \tag{19}$$

The number $n$ depends on the desired precision of the solution. Value of the cuts $\Delta s_i$ on meridional streamline (for the correspond angle $\Delta\chi$) is given by expression (6):

$$\Delta s_i = \frac{r_i c_{mi}}{r_i \omega - c_{ui}}\, \Delta\chi \tag{20}$$

The calculation procedure is performed in an iterative manner as is shown in the previous section.

For the production of the blades and models for its control, it is more convenient to define the blade using its model sections. For this reason, the system of circular planes (lines 0 - 0, 1 - 1,... in Figure 8) is used. The points of intersection of these lines with radial blade sections are defined in a circular plane with radius $r_{ij}$ and angle $\chi_i$.
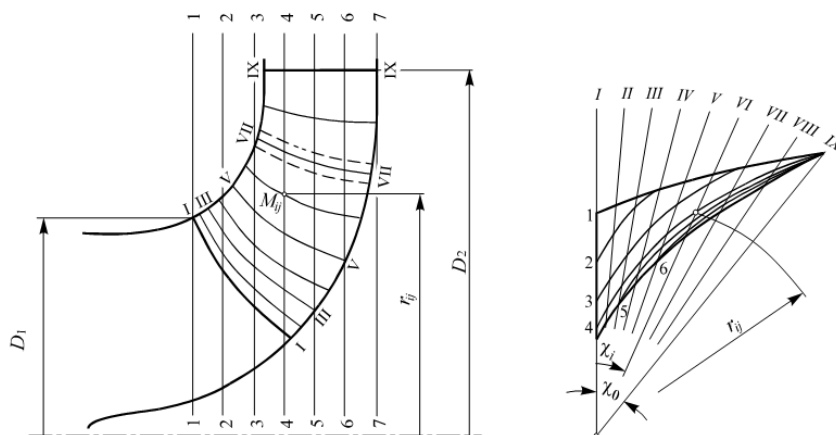


**Figure 8.** Determination of model sections of the impeller blade

Figure 8 shows the impeller blade design for the following basic parameters:
$Y$ = 360 J/kg, $Q$ = 0.3 m³/s, $n$ = 1000 rpm, $D_1$ = 0.27 m, $D_2$ = 0.36 m, $b_1$ = 0.095 m, $b_2$ = 0.055 m.

## 5. CONCLUSION

The solution method developed in the paper, based on free vortex design, involves the linking of meridional and blade-to-blade solutions. The method which employs a finite element techniques has been developed for determining the blade-to-blade flow of an incompressible non-viscous fluid through a rotating turbomachine blade row.

In accordance with Bauersfeld method, the design of impeller blades is performed in iterative manner by using relationships between velocity components and geometrical blade parameters. The applied procedure allows a very fast design of the blade of the hydrodynamic transmissions for the defined input data.

The presented method is shown in case of pump impeller blade, but with minor changes it can be used for the design of the turbine which is the second component of hydrodynamic torque converter.

## REFERENCES

[1] Adibi, A. H., Lashgarian A. N., McPhee, J.: "Modeling Torque Converter Characteristics in Automatic Drivelines: Lock-up Clutch and Engine Braking Simulation", ASME 2012 International Design Engineering Technical Conferences, American Society of Mechanical Engineers, 12PFL / 0362, pp. 359/367, Chicago, 2012.

[2] Mercure, R. A.: "Review of the automotive torque converter", SAE Technical Paper 790046, 1979.

[3] Kotwicki, A. J.: "Dynamic Models for Torque Converter Equipped Vehicles", SAE Technical Paper Series, International Congress and Exposition, Detroit, Michigan, February 22-26, 1982.

[4] Hrovat, D., Tobler, W. E.: "Bond Graph Modeling and Computer Simulation of Automotive Torque Converters", Journal of Franklin Institute, Vol. 319, 1985, pp. 93-114.

[5] Ejiri, E., Kubo, M.: "Performance analysis of automotive torque converter elements," Journal of Fluids Engineering, Vol. 121, No. 2, 1999, pp. 266-275.

[6] Migus, M., Kęsy, A., Kęsy, Z.: "Flow Simulation in Hydrodynamic Torque Converter" Technical Transactions, Mechanics, Vol. 114, No. 7, 2017, pp.165-173.

[7] Jenkins, R. M., Moore, D. A.: "An inverse calculation technique for quasi-three-dimensional turbomachinery cascades," Appl. Math. Comput., Vol. 57, No. 2, 1993, pp. 197–204.

[8] Peng, G.: "A Practical Combined Computation Method of Mean Through-Flow for 3D Inverse Design of Hydraulic Turbomachinery Blades", Journal of Fluids Engineering, Vol. 127, No. 6, 2006, pp. 1183-1190.

[9] Esch, B. P. M., Kruyt, N. P.: "Hydraulic Performance of a Mixed- Flow Pump: Unsteady Inviscid Computations and Loss Models," ASME Journal of Fluids Engineering, Vol. 123, No. 2, 2001, pp. 256-264.

[10] Wu, C. H.: "A General Theory of Three-Dimensional Flow in Subsonic Turbomachines of Radial-, Axial-, and Mixed Flow Types," NACA TN-D2604, 1952.

[11] Peng, G., Fujikwa, S., Cao, S.: "An Advanced Quasi-Three-Dimensional Inverse Computation Model for Axial Flow Pump Impeller Design," Proceedings of the XIX IAHR Symposium-Hydraulic Machinery and Cavitation, H. Brekke et al., eds., World Scientific, Singapore, 1998, pp. 722-733.

[12] Peng, G., Cao, S., Ishizuka, M., Hayama, S.: "Design Optimization of Axial Flow Hydraulic Turbine Runner Part I: An Improved Q3D Inverse Method," International Journal for Numerical Methods in Fluids, Vol. 39, No. 6, 2002, pp. 517–531.

[13] Chen, N., Zhang, F., Li, W.: "An Inverse (Design) Problem Solution Method for the Blade Cascade Flow on Streamsurface of Revolution", ASME Journal of Turbo-machinery, Vol. 108, 1986, pp. 194–199.

[14] Borges, J. E.: "A Three-Dimensional Inverse Method for Turbomachinery: Part 1", ASME Journal of Turbomachinery, Vol. 112, 1990, pp. 346–354.

[15] Chen, N.: "Two- Dimensional Aerodynamic Inverse Problem Solution Study in Turbo-machinery", Hoboken, NJ: John Wiley & Sons, 2010.

[16] Barlit, V.: "Hydraulic Turbomachines" (in Russian), Kiev, 1977.

[17] Kanavagh, P.: „Through-Flow Solution for Axial Turbomachine Blade Rows", Ph. D. thesis, Iowa State University of Science and Technology, 1966.

[18] Chen, C., Zhu, B., Singh, P., Choi, Y.: "Design of a Pump-Turbine Based on 3D Inverse Design Method", Journal of Fluid Machinery, Vol. 18, No 1, 2015, pp. 20-28.

[19] Yang, J., Liu, Y., Wang, X., Wu, H.: "An Improved Steady Inverse Method for Turbomachinery Aerodynamic Design", Journal Inverse Problems in Science and Engineering, Volume 25, No 5, 2017.

[20] Yang, J., Liu, Y., Wang, X., Wu, H.: "An Improved Steady Inverse Method for Turbomachinery Aerodynamic Design", Journal Inverse Problems in Science and Engineering, Volume 25, No 5, 2017.

[21] Andersson B., Andersson R., Hakansson L. et al.: "Computational Fluid Dynamics for Engineers"*,* Cambridge: Cambridge University Press, 2012.

[22] Dmitri K. D., Hämäläinen, J.: "Finite Element Methods for Computational Fluid Dynamics: A Practical Guide", Philadelphia: University City, SIAM-Society for Industrial and Applied Mathematics, 2014.

[23] Milovanovic, D.: "Contribution to the Solution of the Inverse Problem in Hydraulic Turbomachines", MSc thesis, Faculty of Mechanical Engineering, Kragujevac, 1997.

[24] Pfleiderer, C., Peterman, H.: *"Stromungsmaschine",* Springer-Verlag, Berlin/ Gottingen/ Heidelberg, 1964.

# ON THE DESIGN OF THE STEERING AND FRONT UPRIGHTS FOR A RACE CAR

*Greg Wheatley[1*], Caitlin Campbell[2], Ben Moore[3]*

RESEARCH ARTICLE

**ABSTRACT:** Our contribution to fulfil the requirements for the mechanical design project was to audit the existing steering components and design an upright assembly for the JCU Motorsports FSAE car. We were required to assess the current status of the project and pick up where the previous team left off. As undergraduate engineers, we have followed the design process outlined in the assessment criteria issued at the commencement of the project. Many hours of work have been put into the design, material selection and loading analysis to come up with what we believe to be the best design given the constraints and timeline. A major guideline governing the design of the upright housing was the need for it to be reliable. This has been heavily factored into the design and is reflected in the analysis of the load cases giving significant room for errors in calculations and accounting for unforeseen circumstances which can cause significant angst for designers unfamiliar with the field. Overall the requirements of this project have been fulfilled to a high standard. We have taken what we have been given and produced a design to be incorporated into the motorsports project.

**KEY WORDS:** suspension, steering, design, finite element analysis

[1]*Greg Wheatley, PhD, Senior Lecturer, James Cook University, College of Science and Engineering, Townsville QLD 4811 Australia, greg.wheatley@jcu.edu.au (*Corresponding author)*
[2]*Caitlin Campbell, BE, James Cook University, College of Science and Engineering, Townsville QLD 4811 Australia, caitlin.campbell@my.jcu.edu.au*
[3]*Ben Moore, BE, James Cook University, College of Science and Engineering, Townsville QLD 4811 Australia, ben.moore@my.jcu.edu.au*

# O DIZAJNU UPRAVLJANJA I PREDNJIH NOSEĆIH ELEMENATA TRKAČKOG AUTOMOBILA

**REZIME**: Naš doprinos ispunjenju zahteva mehaničkog dela projekta bio je revizija postojećih komponenti upravljanja i nosećih elemenata sklopa automobila JCU Motosports FSAE. Od nas se tražilo da procenimo trenutno stanje projekta i da utvrdimo gde je prethodni tim stao. Kao inženjeri osnovnih studija pratili smo proces projektovanja defisan u kriterijumima za ocenu koji su bili definisani na početku projekta. Mnogo sati rada je uloženo u analizu koncepta, izbor materijala i analizu opterećenja kako bi se došlo do onog za šta verujemo da je najbolje rešenje s obzirom na ograničenja i rokove. Glavna smernica u projektovanju nosača rukavca je bila njegova pouzdanost. Ovo je u velikoj meri implementirano u dizajn i ogleda se u analizi slučajeva opterećenja što daje značajan prostor za greške u proračunu i nepredvidjenim okolnostima koje mogu biti neprijatne za inženjere koji nisu stručni u ovoj oblasti. Sve u svemu, zahtevi ovog projekta su ispunjeni na visokom nivou. Uzeli smo ono što nam je bilo dato i napravili dizajn koji treba ugraditi u projekat moto sporta.

**KLJUČNE REČI:** oslanjanje, upravljanje, dizajn, analiza konačnim elementima

# ON THE DESIGN OF THE STEERING AND FRONT UPRIGHTS FOR A RACE CAR

*Greg Wheatley, Caitlin Campbell, Ben Moore*

## 1. INTRODUCTION

The aim of "Project B - Steering and Front Upright" is to design and build the steering system and front uprights for JCU Motorsports car. To help achieve this goal in the available time, various tasks were set. These include: Research the Formula SAE-A rules to determine restrictions and design requirements; Research on currently used automotive steering systems and evaluation of feasible alternatives; Analysis of previous year team's design; Design an appropriate steering system for the new race car; and Evaluate the performance of the steering system through programs in SolidWorks. The FSAE sports vehicle inter-university competition involves the design and construction of an on-road Open-Wheeler type sports vehicle dictated by FSAE rules and requirements. All James Cook University 3rd year Mechanical Engineering Project B team have the task to continue development of the Open-Wheeler sports vehicle; which was conceived by previous JCU Mechanical Engineering team. There has been little designed, documented or manufactured; and the car has not reached a test worthy phase. The previous team constructed a tubular steel frame, complete engine placement and mounts, seat mounts, a breaking reservoir template and both front and rear suspension [1] wishbones and a simple rack and pinion. Overall; this year's cohort hopes to finish designing most of the components and so that the car might be competing in the following year. Future expectations of the car include; high performance in terms of acceleration, braking and handling qualities as well as high reliability, low cost and easy maintenance. Following are the requirements that have an impact on the design process for steering and uprights. The vehicle is required to be an open-wheeled and open-cockpit design with four wheels not in a straight line. The steering must affect at least two wheels and the allowable free play is limited to 7 degrees total measuring from the steering wheel. The steering system must have positive stops to prevent steering linkages from locking up and to prevent the tires from contacting the car at all times. The allowable free play is limited to 7 degrees total, and is measured at the steering wheel. The Front Hoop must be no more than 250 mms (9.8 inches) forward of the steering wheel and all parts near the driver's legs must be shielded with solid material for safety considerations. The steering wheel, steering column, seat and all padding may be removed during testing. Along with a quick disconnect of the steering wheel attached to the column. The driver must be able to operate the quick disconnect while in the normal driving position with gloves on.

## 2. ANALYSIS

During a high speed racing environment, various common load cases are placed on the vehicle upright assemblies. These load cases have been identified separately and then combined in order to simulate a 'worst case scenario' to obtain an accurate assessment of the loading capacity of the designed upright assembly. To achieve the most accurate analysis of the design, both static and fatigue loading cases have been applied to selected critical components. When available, the dimensions of the current vehicle have been measured in the workshop though due to the current stage of the project, the final mass of the car can only be estimated based on current measurements and designs put forth by other teams in the competition. The following values were used in calculating the load cases:

| | |
|---|---|
| Mass of Car | M = 350 kg |
| Centre of Mass | (x, y, z) = (931, 279, 197)   mm |
| Wheelbase | l = 1715 mm |
| Minimum turning radius | r = 3512 mm |
| Coefficient of friction (rubber on asphalt) | c = 0.8 [2][3] |

Case one will find the forces on each of the uprights due to both acceleration and deceleration. Both conditions have been considered and it is expected that there will be greater force on the rear uprights during acceleration and greater force on the front uprights during deceleration. For this load case constant acceleration/deceleration has been assumed and an estimate made of the vehicle basic force analysis and moment analysis has been used to generate the following loads. From this the vertical forces on the front and rear uprights are:

$$F_{front} = \frac{1}{2}mg\frac{a_2}{l} - \frac{1}{2}mg\frac{ha}{lg} \tag{1}$$

$$F_{rear} = \frac{1}{2}mg\frac{a_2}{l} + \frac{1}{2}mg\frac{ha}{lg} \tag{2}$$

From the current geometry of the previous FSAE car the dimensions are as follows;
M = 350Kg, $a_1$ = 851mm, $a_2$ = 864mm, h = 440mm,  g = 9.81m/s$^2$, l = 1715mm
a = acceleration of car.

The acceleration of the car has been estimated at 0.9g, meaning the time taken to accelerate from standing to 100 km/h would be approximately 3.1 seconds.  This acceleration value has been obtained through research of other FSAE cars and represents an idealised performance of the JCU car.

$$a = 0.9g = 8.829 \frac{m}{s^2}$$

$$F_{front} = \frac{1}{2}(350)(9.81)\frac{864}{1715} - \frac{1}{2}(350)(9.81)\frac{440 \, x \, 8.829}{1715 \, x \, 9.81} = 468.48 \text{ N} \tag{3}$$

$$F_{rear} = \frac{1}{2}(350)(9.81)\frac{851}{1715} + \frac{1}{2}(350)(9.81)\frac{440 \, x \, 8.829}{1715 \, x \, 9.81} = 1248.27 \text{ N} \tag{4}$$

The results show that when the car is accelerating there is a higher vertical force on the rear upright than there is on the front upright. The deceleration of the car has been estimated at 1.3g, meaning the time taken to get the car to stop completely from a velocity of 100 km/h would be just under 2.2 seconds. Again this is an idealised case though perhaps more realistic as the deceleration of the car depends heavily on the performance of the brakes and not power output of the engine.

$$a = 1.3g = 12.753 \frac{m}{s^2}$$

$$F_{front} = \frac{1}{2}(350)(9.81)\frac{864}{1715} - \frac{1}{2}(350)(9.81)\frac{440 \, x - 12.753}{1715 \, x \, 9.81} = 1437.47 \text{ N} \tag{5}$$

$$F_{rear} = \frac{1}{2}(350)(9.81)\frac{851}{1715} + \frac{1}{2}(350)(9.81)\frac{440 \, x - 12.753}{1715 \, x \, 9.81} = 279.29 \text{ N} \tag{6}$$

The results show that when the car is decelerating there are higher forces on the front upright than there is on the rear. This case refers to the roll of a vehicle when turning. It is very hard to model in a 3D dynamic situation however is easy to model at its extremes. When the car is turning, there is a tendency for the car move away from the centre of the turning radius known as centripetal forces. Because the wheels are constraining the car and the centre of mass is above the ground, will be inclined to roll. It can be assumed at an extremity that the FSAE car's inside wheels will apply a zero force to the track and potentially lift off the ground during a hard corner, subsequently the centripetal forces and also weight of the car will be acting through 2 uprights (outside front and rear). The vertical forces acting on the car at the point of wheel lift is as follows:

$$F_{inner} = \frac{1}{2}mg \tag{7}$$

$$F_{outer} = 0 \tag{8}$$

Solving these equations given a car mass of 350Kg results in:

$$F_{inner} = 1716.75 \text{ kN} \tag{9}$$

$$F_{outer} = 0 \text{ N} \tag{10}$$

Because the car is in a rolling motion there is also a bending force on the inner front and rear uprights. This causes a moment on the hub shaft and the supporting bearings [4]. Because of the difference in upright geometry and bearings [5] in each upright the torsion force must be divided into two parts; one for the front upright and another for the rear.

The front upright hub shaft is supported by two bearings [6] 27mm apart and 14mm each wide. The $F_{inner}$ can be applied to the hub shaft bolts and resolved into two reaction forces contained on the upper and lower half at each bearing [7]. The followings equations were used to resolve the forces:

$$\sum M_{shaft} = 0 \tag{11}$$

$$\sum F_{shaft} = 0 \tag{12}$$

Where the sum of the moments about the shaft are equal to zero and the sum of the forces on the shaft is also equal to zero. The forces at each bearing [8] have been calculated as:

$$F(R_{b1}) = 2509.1 \text{ N} \tag{13}$$

$$F(R_{b2}) = -792.3 \text{ N} \tag{14}$$

The brake calliper mounts on both the front and rear uprights are offset from the centre of rotation of the hub shaft. This means, when the car is braking, the upright in question will resist the braking force and thus experience torsion in slowing the car's velocity.

The force required to stop the car at a rate of 1.3g:

$$F = ma = 350 \ x \ (9.81 \ x \ 1.3) = 4464 \text{ N} \tag{15}$$

This force can then be converted into a torque using the radius of the wheel:

$$T_t = F \cdot r_w$$

$$T_t = 4464 \, x \, 0.25 \ = 1116 \, \text{Nm} \qquad (16)$$

This is the torque required to stop the car, this torque will be distributed between the four uprights of the car. The FSAE rules state that the front brakes must be able to apply a force capable of stopping 100% of the car, and the rear brakes must be able to stop 60% of the car. The front uprights must then be able to resist a torque of:

$$T_t = 1116 \, \text{Nm} \qquad (17)$$

$$T_{fw} = 558 \, \text{Nm} \rightarrow \text{force per front wheel} \qquad (18)$$

The torque on each the wheel can then be resolved into a force acting at brake calliper bolt holes in a direction which is tangent to the pitch circle diameter:

$$F_{PCD} = T_{fw} \, x \, r_{PCD}$$
$$F_{PCD} = 558 \, x \, 0.092 \ = 51.336 \, \text{N (Caliper Holes Total)} \qquad (19)$$

Two bolts keep the calliper in position. It is assumed that the force is distributed equally between them resulting in a force per hole of $F_{hole}$ = 25.7 N. Intuitively, the force on the rear upright mounts is 60% of this assuming a common pitch circle diameter. Another force common to racing is that of hitting a bump at high speed which is prone to any of the wheels of the car. Unlike the other cases it is very hard to quantify the amount of force on the uprights when the car hits a bump in the road. In some instances this case can be disregarded under the assumption that the FSAE car is designed for on road use, where bumps are uncommon and can be neglected. However, due mainly to the fact that the JCU FSAE motorsports team is still in the early stages of designing a car and has very limited prior experience the case will be included to account once again for a 'worst case scenario'. FSAE forums and other literature suggest that the force on the upright due to a bump in the road is three times the mass of the car. The bump force equation has been generated assuming that the cars weight is distributed evenly by the four uprights due to lack of knowledge on the mass distribution of the finished car and the force distribution at the time of the bump. The current calculation for the centre of mass dictates that there will be 156 kg supported by the front two wheels meaning that this assumption is not a conservative underestimate of this weight.

$$F_{front} = 3 \, mg = 3 \, x \, \frac{350}{4} \, x \, 9.81 = 2675.125 \, \text{N} \qquad (20)$$

$$F(R_{b1}) = 5048 \, N \qquad (21)$$

$$F(R_{b2}) = -2423 \, N \qquad (22)$$

When taking into account cornering forces we look back into basic system dynamics [9]. If a car is taking a corner as fast as it possibly can, then the friction force will be the same as the normal force, which is the basis of the calculation. When the car begins to slip the forces on the upright will decrease, therefore the critical point when the forces are highest on the upright is the point just before slipping occurs. Thus when the traction force is equal to the normal component of force, there is the highest amount of force on the uprights. The diagram below shows how the normal component of force is calculated.

$$F_{traction} = F_{normal} \qquad (23)$$

$$cmg = ma_n \tag{24}$$

$$cg = a_n \tag{25}$$

$$a_n = 7.848 \; \frac{m}{s^2} \tag{26}$$

We also know that the acceleration in the normal direction can be resolved into an angular velocity:

$$a_n = \omega^2 r \tag{27}$$

$$\omega = 1.5 \; \frac{rad}{s} \tag{28}$$

$$V = \omega r = 1.5 \; x \; 3.5 \; = 5.241 \; \frac{m}{s} \approx 20 \; \frac{km}{h} \tag{29}$$

$$|F_r| = \frac{1}{2} m \frac{V^2}{r} \tag{30}$$

$$|F_r| = \frac{1}{2} (350) \frac{(5.241)^2}{3.5} = 1373.4 \text{ N} \tag{31}$$

This is the theoretical force exerted on the uprights due to cornering. Though the case is highly simplified, it provides an estimate of the forces during cornering without the use of complex 3D modelling. A total of 5 individual loading conditions on the upright assembly have been identified. Of these, two combined loading case scenarios will be used for analysis to achieve an extreme loading condition for each of critical parts of the assembly. The upright housing and hub shaft will have two load cases applied and will be analysed in both static and fatigue conditions to ensure longevity. The first set of load cases takes into consideration a regular combination on the racing track whereby the vehicle is entering a corner at high velocity and so the driver is slowing down at maximum deceleration into a corner. In this case, there is torsion on the upright housing due to the brake callipers, a high deceleration force on the front uprights and also a cornering force. The second load case of a bump was applied to both the upright housing and the hub shaft. Though practically an uncommon occurrence on a smooth racing track, they were taken into account to ensure the upright design components can withstand the forces. The load case applied to the steering anchor was half of the force due to cornering, as there are two wishbone supports, as well as the maximum force calculated for steering in the direction of the steering arm. For this component only a heavy corner would apply the maximum loading conditions which have been considered. Loading on the bearing [10] cap was taken to be the full force of the cornering load in the event that there is catastrophic failure of the bearings [11] and the entire load is applied to the cap which would essentially be holding the hub shaft in the bore of the main housing. It is important that this component be strong enough to withstand these forces as it could prevent the wheel detaching from the car in the event of a crash. As with the bearing [12] cap, the shaft retainer was also assessed under the full load assuming catastrophic bearing failure. Two sets of loading cases were applied to the upright housing.
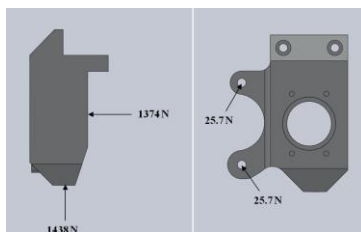
**Figure 1.** Deceleration, Braking and Cornering load case on upright housing
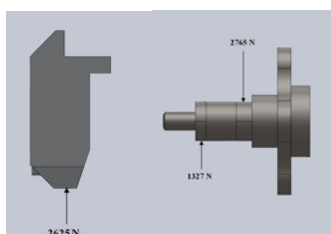


**Figure 2.** Bump load case on upright housing (L) Deceleration, Braking and Cornering load case on hub shaft (R)

For each load case applied to the upright housing, the magnitude and direction of the forces is indicated in the figures 1 and 2. The brake calliper forces were applied to the holes at a direction tangent to the pitch circle diameter and the other forces applied to the circular bore where the bearings would contact both normal and parallel to the surface. The fixture was added to the holes at the bottom wishbone support bolt hole and the holes at the top where the steering anchor bolts to the upright housing.
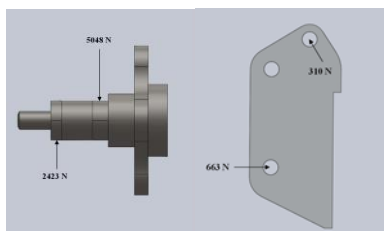


**Figure 3.** Bump load case on hub shaft (L) Deceleration, Braking and Cornering load case on steering anchor (R)

The loads on the hub shaft have been applied at the upper and lower halves of the shaft where the bearings make contact. The bearings are self-aligning and can thus allow for any curvature in the shaft due to moments. The fixtures were added to the bolt holes where the wheel would bolt on to allow for accurate simulation of how the bearings would behave under loading thus not restricting completely the bending motion of the shaft. The forces on the steering anchor were applied to the top wishbone contact point and the steering arm bolt hole. The restraints for the anchor were the holes which are used to bolt to the upright housing.
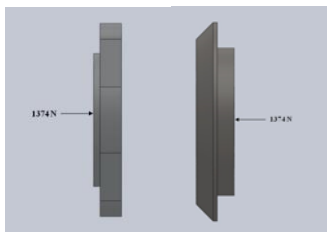
**Figure 4.** Deceleration, Braking and Cornering load case on bearing cap (L)
Deceleration, Braking and Cornering load case on shaft retainer (R)

The bearing cap loading was applied to the face where the bearings could push on the face. The restraints where positioned at the holes holding the cap to the upright housing. The force applied to the shaft retainer was at the contact point with the bearing inner race. The restraint for the shaft retainer was located on the opposite side at a circle approximately equal to the size of the bolt head holding the retainer to the hub shaft. Selection and placement of the upright hub/shaft bearings requires calculations to determine selection is correct and bearings are capable of withstanding maximum forces applied during a racing event. Maximum forces applied to the RHF upright include a combination of loads during a race [13] event such as heavy cornering to the left, hard braking and a 'bump' impact. Analysis on the forces inflicting the RHF upright hub/shaft are depicted in figure 3 and illustrate the loads applied at particular locations. The force applied to the right-hand angular contact bearing supports the highest load and is therefore the point of interest for analysis. NTN supplies formulas and loads allowable to determine the actual loads applied to the bearing. The formula incorporates a load factor fw and is obtained by bearing manufacture Data Sheets as per Appendix 00. The maximum permissible dynamic load applied to the bearing is 17 500N. Calculating the Actual Load to bearing is fw x Applied Load = Actual Load, 1.5 x 4795N = 7192.5N. Therefore, Factor of Safety for NTN 7007 Angular Contact Bearing is

$$F_oS = \frac{17500}{7192.5} = 2.43 \tag{32}$$

Referencing the textbook 'Applied Mechanical Design', 1986 regarding Factor of Safety of 2 is recommended for general basic endurance applications. The NTN 7007 Angular Contact bearing is recommended and safe for use within the FSAE Sports Vehicle front upright housings. Performing an analysis on the designed hub/shaft with a current diameter of 35mm, at bearing locations, it is assumed the location enduring the highest stress concentration will be at the step in shaft diameter on the right bearing. Complying with AS1403-2004 'Design of Rotating Steel Shafts', formula 33 has been selected due to the required criteria. The formula is:

$$D_3 = \frac{10^4 \cdot F_s}{F_r} \sqrt{\left[K_s \cdot K \cdot \left(M_q + \frac{P_q \cdot D}{8000}\right)\right] + \frac{3}{4}T_q{}^2} \tag{33}$$

Subbing values for all the variables include:

$F_s = 2$ ($F_oS$); factor of safety

$\quad M_q = 2600N \cdot 0.038m = 98.8Nm$ Movement at the investigated point

$\quad K_s = 1.325$; Surface

K = K4 + K6 = 1.9 + 2.7 = 4.6; the summation of aspect ratio (shafts)

$P_q$ = 0; normal

$T_q$ = 0; torque

$F_r$ = Sn'· CL · CG · CS · CT · CR = 0.5 · 1020 · 1 · 0.9 · 0.8 · 1 · 0.753 = 276 MPa (Fatigue or endurance limit).

D = 26mm minimum required. Current shaft diameter is 35mm which is safe for use as per AS1403-2004.

Manual fatigue analysis was undertaken on the upright housing and the hub shaft. The following equation was used in order to obtain a figure for the safety factor:

$$\frac{\sigma_a}{S_{fn}} + \frac{\sigma_m}{S_{ut}} < \frac{1}{N} \tag{34}$$

Where

S$fn$ = Fatigue Strength (Endurance Limit)

S$ut$ = Ultimate Tensile Strength

N = Safety Factor

**Table 1.** Endurance calculations for the hub shaft and upright housing materials

| Factor | | Hub Shaft AISI 4140 CS | Upright Housing 2024 T3 Al Alloy |
|---|---|---|---|
| Ultimate Tensile Strength (MPa) | $S_u$ | 1140 | 428 |
| R.R. Moore Endurance Limit (MPa) | $S_e'$ | 570 | 171.2 |
| Load Factor | $C_L$ | 1 | - |
| Gradient Factor | $C_G$ | 0.9 | - |
| Surface Factor | $C_S$ | 0.8 | - |
| Temperature Factor | $C_T$ | 1 | - |
| Reliability | $C_R$ | 0.753 | - |
| Endurance Limit (MPa) | $S_{fn}$ | 309 | 138 |

**Table 2**. Estimated safety factors for fatigue of the hub shaft and upright housing materials

| Factor | | Hub Shaft AISI 4140 CS | Upright Housing 2024 T3 Al Alloy |
|---|---|---|---|
| Mean Stress | $\sigma_a$ | 0 (Fully Reversed) | 0 (Fully Reversed) |
| Stress Amplitude | $\sigma_m$ | 5048 | 1438 |
| Fatigue Strength | $\sigma_{fn}$ | 309000000 | 138000000 |
| Ultimate Tensile Strength | $\sigma ut$ | 1140000000 | 428000000 |

| Safety Factor | 1/N | 1.63366E-05 | 1.04203E-05 |
| Maximum Safety Factor | N | 61212.36133 | 95966.62031 |

For each of the materials, the safety factor has been calculated using the formula. Each of the metals is clearly strong enough to withstand the required loading effects applied to the upright assembly even though unrealistic fatigue cases have been applied to each. The hub shaft has been assessed at a bump force fatigue loading fully reversed and the upright housing has been assessed for normal expected deceleration, braking and cornering load case also fully reversed.
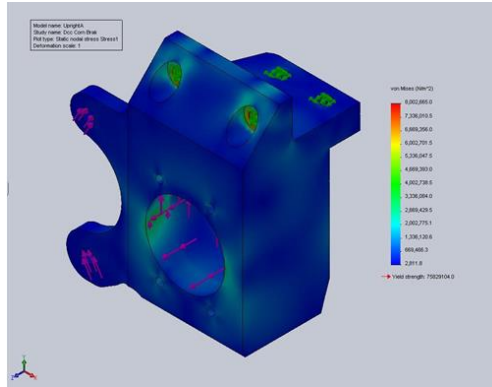


**Figure 5.** FEA Deceleration, Braking and Cornering load case on upright housing - Max Stress: 8 MPa, 75.8 Yield Stress: MPa, Safety Factor: 9.5
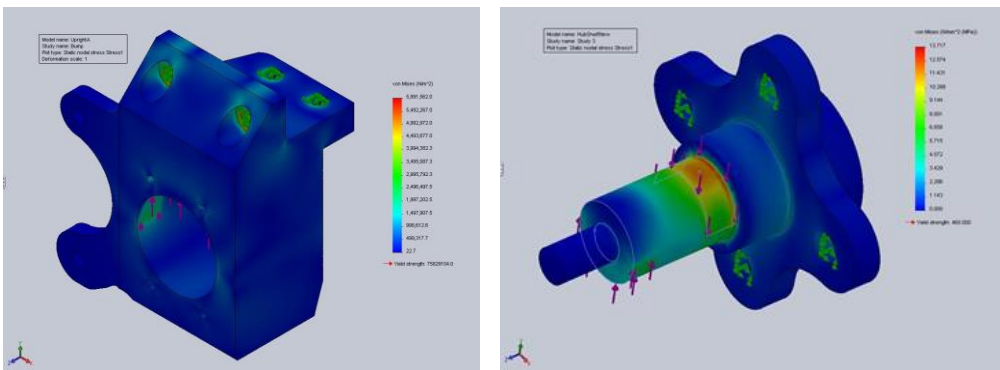


**Figure 6.** FEA bump load case on upright housing - 5.99 Max Stress: MPa 75.8 Yield Stress: MPa, Safety Factor: 12.65 (L) FEA Deceleration, Braking and Cornering load case on upright housing - Max Stress: 13.7 MPa, Yield Stress: 460 MPa, Safety Factor: 33.6 (R)
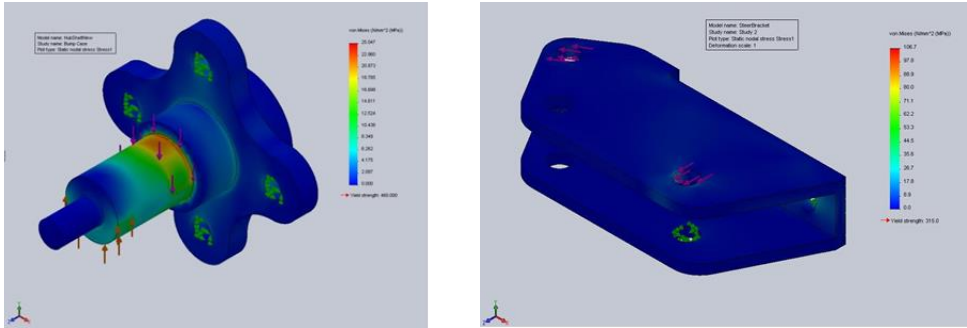
**Figure 7.** FEA bump load case on upright housing - Max Stress: 25 MPa, Yield Stress: 460 MPa, Safety Factor: 18.4 (L) FEA cornering and steering load case on upright housing - Max Stress: 106.7 MPa, Yield Stress: 315 MPa, Safety Factor: 2.95 (R)
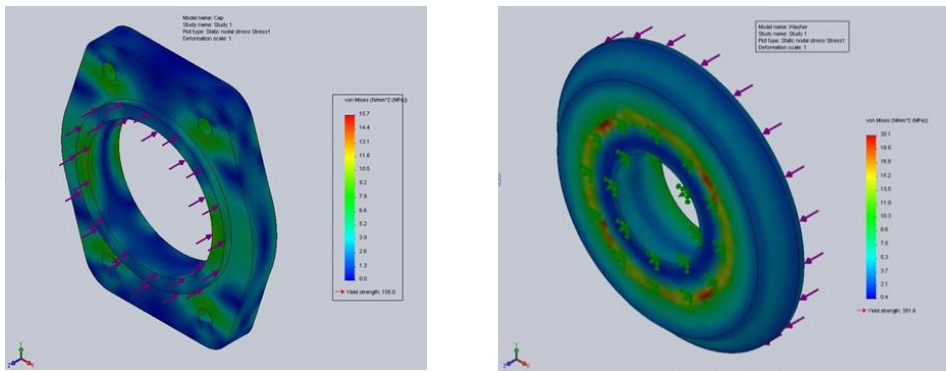


**Figure 8.** FEA cornering load case on upright housing - Max Stress: 15.7 MPa, Yield Stress: 105 MPa, Safety Factor: 6.7 (L) FEA cornering load case on upright housing – Max Stress: 20.1 MPa, Yield Stress: 351.6 MPa, Safety Factor: 17.5 (R)
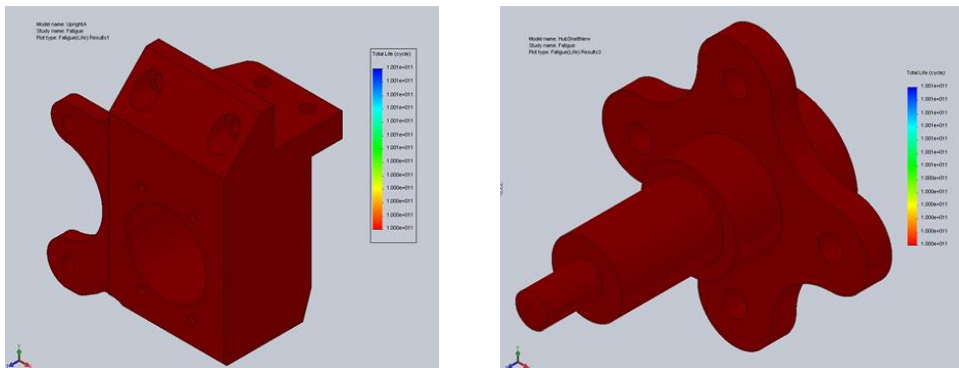


**Figure 9.** FEA Deceleration, Braking and Cornering fatigue load case on upright housing for infinite life (L) FEA Deceleration, Braking and Cornering fatigue load case on hub shaft for infinite life (R)

Using Eulers formula adapted to a cylinder you attain:

$$P_{cr} = \frac{\pi^2 \cdot E \cdot I}{Le^2} \qquad (35)$$

Where I is the inertia $= \frac{\pi \cdot d^2}{64}$; and Youngs modulus is 690 GPa. The $L_e = 180$mm, $P_{cr} = 288725$ N. Therefore the amount of force that the Aluminium protectors can handle is 288.725 kN which is over the amount of force being applied from the tyres. Due to the steering system being made of material higher than the given critical force; the steering system won't be considered for a full static analysis and will only incorporate changes in the steering arm components or rack protector. The different components of the assembly will be applied forces such as axial forces i.e. tensile and compressive force and also shear forces. The force acting on the assembly is cornering force which is being calculated 660 N.

The finite element analysis of the components is done using Solidworks simulation and the results are shown below. The connecting arm will be mainly applied to axial forces i.e. tensile and compressive force. The yield strength of the material used for the connecting arm is 220 MPa. The Solidworks force analysis simulation done on this part is shown in the figure below.
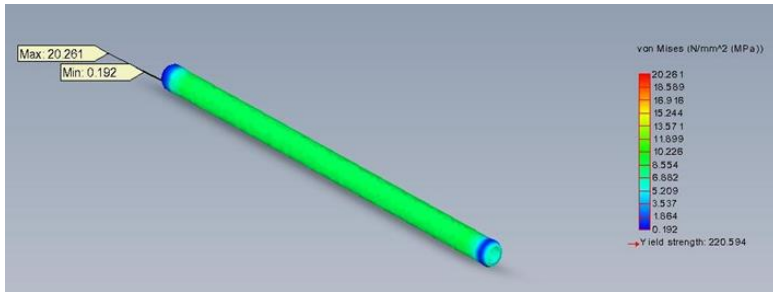


**Figure 10.** Connecting rod in tension

The simulation shows that the minimum FOS for this design is 10. And the maximum stress produced in the rod is 20 MPa which is much lower than allowable stress so the design is safe. The tie rod is also applied to axial forces. The critical forces acting on the tie rod is at threads. The shear force at the thread face, the tension at the bottom of the thread. And also the crushing at the top of the threads. The Solidworks simulation done on the tie road is shown below.
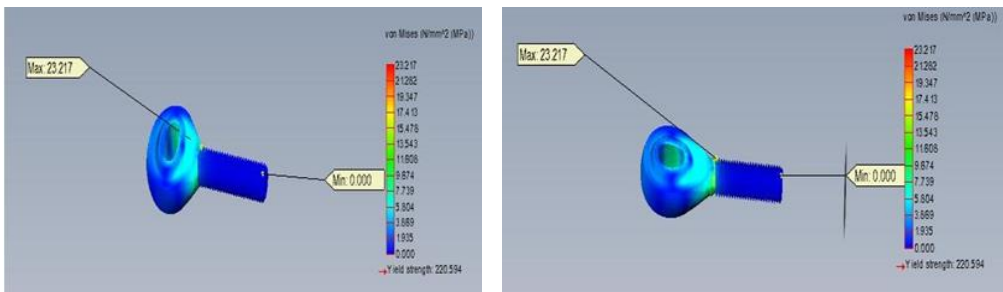


**Figure 11.** Tie rod in compression (L) Tie rod in tension (R)

We can observe from the simulation that the maximum stress produced during axial loading on the tie rod end is 23.217 MPa and the minimum FOS for the component we used is 9.5. Clevis will be applied to axial force as well. During compression the force will act on the face of the clevis by the extension rod and during tension the force will be applied to the clevis by the hexagonal cap screw. The simulation of the force analysis using Solidworks is shown below.
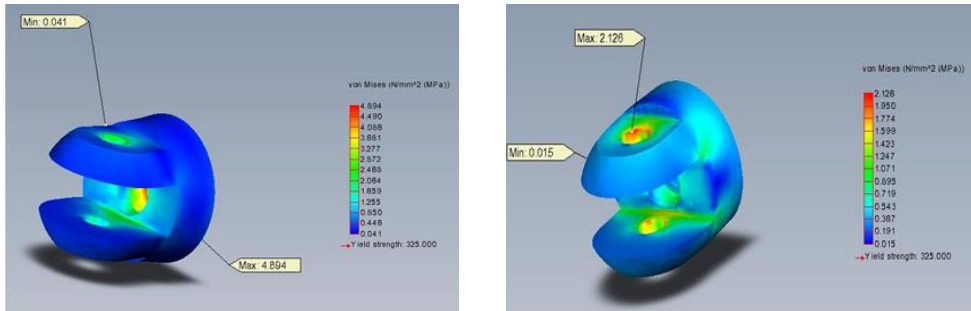


**Figure 12.** Clevis under axial loading

The simulation shows that the minimum FOS of the component while applied load is 66. And the maximum stress produced is 4.89KPa. This screw will also subject to axial loading. The simulation data is shown below. The screw will be subjected to tensile force only.
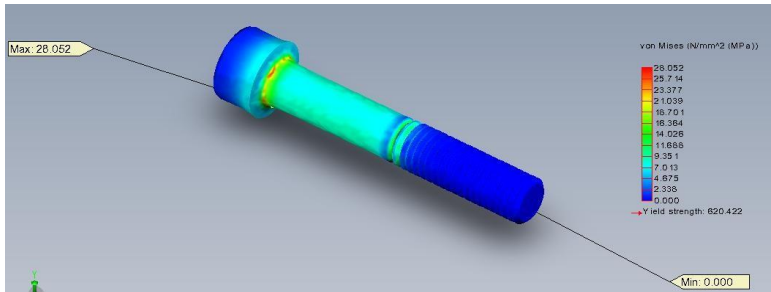


**Figure 13**. Hexagonal socket head cap screw applied to tensile load

From the simulation we can see that the maximum stress induced in the part will be 28.05 MPa and the minimum FOS is 22 for the used screw. There are two bolts used in the assembly one is to connect clevis to the connection arm and the other is to connect the upright to the arm. At both the places the screw will be applied to the double shear. The shear force induced in the hexagonal bolt is,

$$\tau = \frac{P}{2A} = \frac{660}{\frac{\pi}{4}(0.0095)^2} = 4.65 \; MPa \tag{36}$$

Analytically the minimum FOS is 137. So the hexagonal bolt we used is also safe in double shear. When observing the rack protector on the previous design; the load being translated through the protectors would be concentrated at the end of the shaft. Applying the load of 660 N to the ends of the shaft and observing the safety factor and deformation of the shaft.
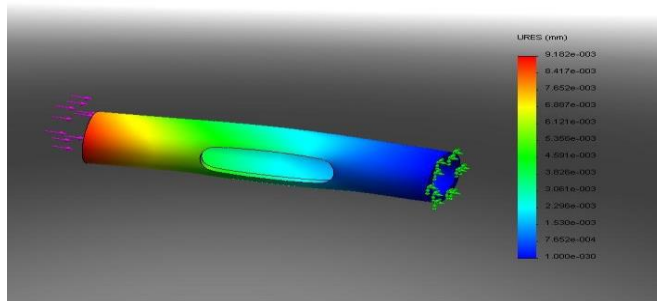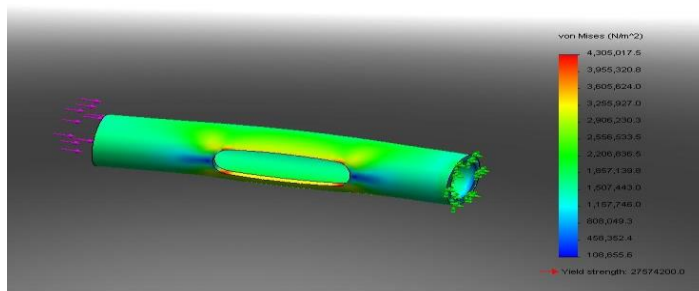
**Figure 14.** Deformation on the shaft



**Figure 15.** Von Misses Stress on the shaft

As it can be seen in the FEA results; the shaft attains minimal deformation and a common stress of 1.15 MPa throughout the shaft. When comparing the stress against the yield strength 27.5 MPa for aluminium; it can be seen that the shafts stress is less. However to make sure the design is able to withstand repeated loading and infinite the life; the shaft is modified with a thicker diameter at the ends. This is checked against with FEA simulation and the changes in the stresses and deformation are observed.
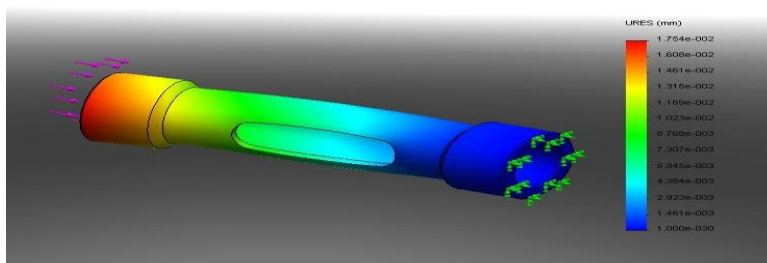


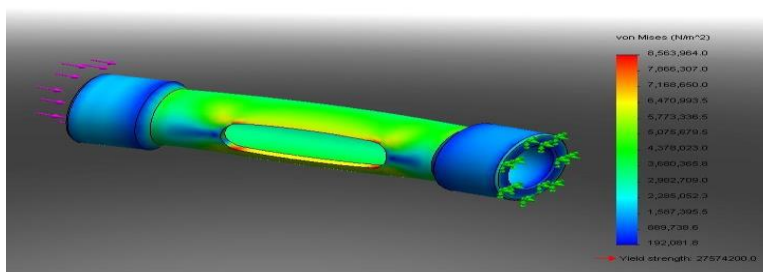**Figure 16.** Deformation on the modified shaft

**Figure 17.** Von Misses Stress on the shaft

Even though the modified shaft has increased the stresses recorded in the middle of the shaft; it has minimized the deformation and has created stable ends which are constantly impacted on throughout the design's life.

## 3.   CONCLUSION

Our contribution to fulfil the requirements for the mechanical design project was to audit the existing steering components and design an upright assembly for the JCU Motorsports FSAE car. We were required to assess the current status of the project and pick up where the previous team left off. As undergraduate engineers, we have followed the design process outlined in the assessment criteria issued at the commencement of the project. Many hours of work have been put into the design, material selection and loading analysis to come up with what we believe to be the best design given the constraints and timeline. A major guideline governing the design of the upright housing was the need for it to be reliable. This has been heavily factored into the design and is reflected in the analysis of the load cases giving significant room for errors in calculations and accounting for unforeseen circumstances which can cause significant angst for designers unfamiliar with the field. Overall the requirements of this project have been fulfilled to a high standard. We have taken what we have been given and produced a design to be incorporated into the motorsports project.

## REFERENCES

[1]   Allan S.: 'Competition Car Suspension', 2006.
[1]   Machinerys HandBook, 27th Edition, 2007.
[2]   http://www.engineershandbook.com/Tables/frictioncoefficients.htm.
[3]   http://www.skf.com/skf/productcatalogue/jsp/viewers/imageViewerJs.jsp?image=b earingselection.jpg&file=1_0_2&maincatalogue=1&lang=en.
[4]   http://www.skf.com/portal/skf/home/products?maincatalogue=1&lang=en&newlin k=1_3_13.
[5]   http://www.skf.com/portal/skf/home/products?maincatalogue=1&lang=en&newlin k=1_3_4.
[6]   http://www.skf.com/skf/productcatalogue/jsp/viewers/productTableViewer.jsp?tabl eName=1_3_1&maincatalogue=1&lang=en.
[7]   http://www.skf.com/skf/productcatalogue/Forwarder?action=PPP&lang=en&imperi al=false&windowName=null&perfid=123006&prodid=1230060307.

[8] http://www.skf.com/portal/skf/home/products?maincatalogue=1&lang=en&newlink=1_3_25.

[9] Thomas, D. Gillespie: 'Fundamentals of Vehicle Dynamics', 1992.

[10] http://www.skf.com/skf/productcatalogue/Forwarder?action=PPP&lang=en&imperial=false&windowName=null&perfid=125010&prodid=125010407.

[11] http://www.nsk.com/products/ballbearing/angularcontact/pdf/NSK_CAT_E1102h_B46-B75.pdf.

[12] http://www.tec.nsk.com/Handbook.asp?menu=7,0,0,0&PageID=/FitsAndInternalClearances/RadialBearingAndHousingBores.html.

[13] http://www.tec.nsk.com/Handbook.asp?menu=7,0,0,0&PageID=/FitsAndInternalClearances/RadialBearingsAndShafts.html.

[14] http://www.revolutionracegear.com.au/index.php?PCID=10546&PSO=245&PSID=635661&PSV=Primary&CDO.

*Intentionally blank*

# MANUFACTURING SPECIFICITY OF VEHICLE'S INDEPENDENT SUSPENSION SYSTEM PARTS

*Vladica Živković[1], Bogdan Nedić[2*], Stefan Đurić[3]*

RESEARCH ARTICLE

**ABSTRACT:** Independent suspension system of a vehicle allows vertical movements of a wheel, without it affecting the other wheel of the same axle, unlike the solid one. Many elements of the independent suspension systems have been made out of steel in the past, but are recently being replaced by other new materials. Achieving top quality and short cycle times of machining, along with minimising cost per piece have always been key goals for mechanical engineers for technology. Many cutting tool manufacturers make recommendations regarding the selection of machining operations and tools for a range of automotive industry components. These recommendations are presented in this paper and should be kept in mind when designing the technology.

**KEY WORDS:** vehicle, independent suspension, cutting tool, machining

[1]*Vladica Živković, PhD student, University of Kragujevac, Faculty of Engineering, Sestre Janjić 6, 34000 Kragujevac, Serbia*
[2]*Bogdan Nedić, PhD prof., University of Kragujevac, Faculty of Engineering, Sestre Janjić 6, 34000 Kragujevac, Serbia, nedic@kg.ac.rs  (\*Corresponding author)*
[3]*Stefan Đurić, MSc, University of Kragujevac, Faculty of Engineering, Sestre Janjić 6, 34000 Kragujevac, Serbia, sdjuric@kg.ac.rs*

# SPECIFIČNOSTI PROIZVODNJE DELOVA SISTEMA NEZAVISNOG OSLANJANJA VOZILA

**REZIME**: Nezavisni sistem oslanjanja kod vozila omogućava nezavisno vertikalno pomeranje točkova, bez međusobnih uticaja, za razliku od zavisnog sistema oslanjanja. Mnogi elementi nezavisnih sistema oslanjanja izrađivani su od čelika u prošlosti, ali ih u poslednje vreme zamenjuju drugi novi materijali. Postizanje vrhunskog kvaliteta i kratko vreme ciklusa obrade uz minimiziranje troškova, su uvek bili ključni ciljevi inženjera - tehnologija. Mnogi proizvođači reznih alata daju preporuke za izbor postupaka obrade pojedinih delova za automobilsku industriju. Te preporuke za izradu delova sistema nezavisnog oslanjanja su prikazane u ovom radu i treba ih imati na umu prilikom projektovanja tehnologija izrade.

**KLJUČNE REČI:** vozilo, nezavisno oslanjanje, rezni alat, obrada rezanjem

# MANUFACTURING SPECIFICITY OF VEHICLE'S INDEPENDENT SUSPENSION SYSTEM PARTS

*Vladica Živković, Bogdan Nedić, Stefan Đurić*

## 1. INTRODUCTION

Independent suspension system of a vehicle allows vertical movements of a wheel, without it affecting the other wheel of the same axle (Figure 1), unlike the dependent one. Most passenger vehicles and light trucks are equipped with an independent suspension system on the front axle, which provides a greater amount of engine space, greater wheel displacement, better vibration resistance, and overall better ride comfort, in comparison with the dependent system [9, 10].

The main disadvantages of this system are the complexity of the construction and the cost of production, due to the increased number of parts. Of course, the independent suspension system can be applied to the rear axle of the vehicle [18].
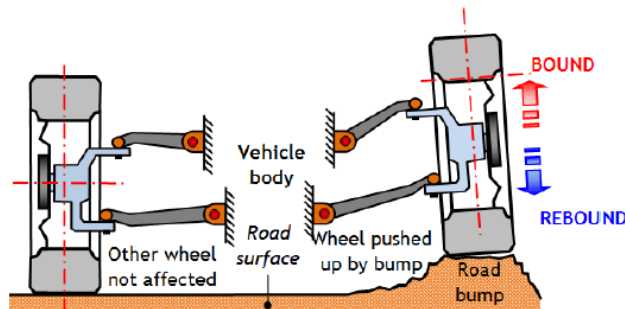


**Figure 1.** Independent suspension system (front view) [1]

There is a number of different types of independent suspension systems that are used:

- MacPherson suspension system
- Double wishbone suspension system
- Multi-link suspension system and
- Trailing arm.

The MacPherson suspension consists of a control arm and strut shock absorber assembly (damper and coil spring) which allow the wheel to move vertically. The main components of the system are shown in Figure 2a. It can be used on both the front and rear axle of the vehicle. Use of this suspension type results in reduced number of parts compared to other types of independent suspension, less weight and greater ride comfort. The key disadvantages include the requirement of additional space in vertical direction and lower levels of adaptability and performance.
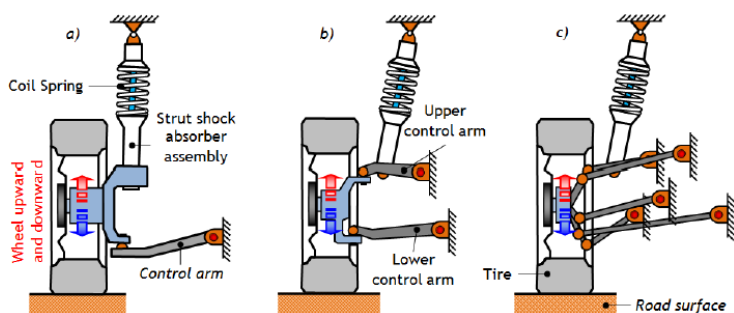
**Figure 2.** Different types of independent suspension system [2]

a) MacPherson suspension, b) Double wishbone suspension, c) Multi-link suspension

Double wishbone suspension system consists of two control arms, upper and lower, which are often called *a-arms* or *wishbones*, due to their shapes. It is mostly implemented in luxury and sport vehicles, as it provides a favourable compromise between vehicle handling and comfort. It consists of two control arms that prevent tilting of the wheels (Figure 2b). The control arms usually are of different lengths, with the lower one being longer.

The leading advantage of this type of suspension is an increase of negative camber, which is a direct consequence of vertical movements of the upper and lower arms. This has a positive effect on the stability of the vehicle, as the outer wheels maintain better contact with the surface during cornering. The disadvantage compared to other solutions is the complexity of the construction, the cost of production, the increased number of parts such as joints and bearings, which increase wear of tires. Multi-link suspension system possesses three or more lateral and one or more longitudinal control arms, which have different lengths (Figure 2c). This system offers a good compromise between comfort, stability and handling. The advantage is that certain parameters of this system can be adjusted without affecting the entire assembly. However, this system is more complex and expensive than others. When it comes to off-road vehicle applications, the disadvantage is that it does not provide sufficient vertical wheel movement.

Figure 3 presents the double wishbone suspension system produced by ZF.



**Figure 3.** ZF double wishbone suspension [3]

Figure 4 gives an example of an independent suspension as a major component of a driveline system for high-mobility vehicles, suitable for fast light-duty vehicles and heavy

Armoured Personnel Carrier (APC) or Mine Resistant Ambush Protected vehicles (MRAP) [12].



**Figure 4.** Independent suspension axles for high mobility vehicle [12]

## 2. INDEPENDENT SUSPENSION COMPONENTS MANUFACTURING

### 2.1 Forming of independent suspension components

Before observing forming and machining processes for independent suspension components, it is necessary to select materials which will be used. During the selection of the materials, it is crucial to take into account that the selected materials must allow smooth driving on different terrains, during high accelerations, sudden braking and other more extreme situations. Very important factor is also the lifetime of elements, which should range from 107 to 108 driving cycles versus a defined stress loading and stiffness criteria.

Many elements of the independent suspension systems have been made out of steel in the past, but are recently being replaced by other materials, such as compacted graphite cast iron (CGI), spheroidal graphite iron (SGI), and magnesium/aluminium alloys, which significantly contribute to weight loss [4]. Examples of different independent suspension constructions are shown in Figure 5 [11].
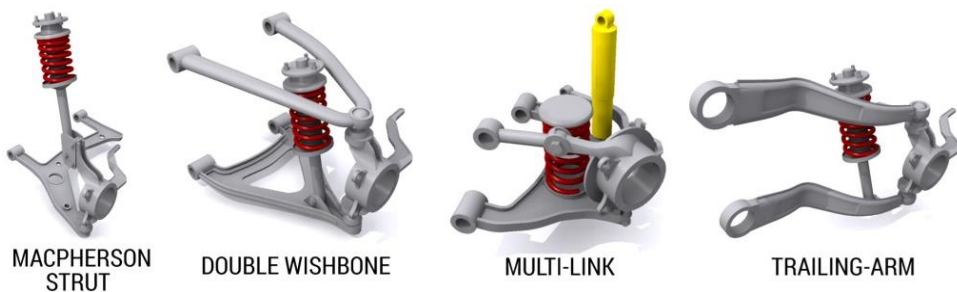


**Figure 5.** Examples of different independent suspension constructions [11]

Depending on the selected material, thickness of the element and the available accommodation space, it is decided whether the element will be forged or casted. Forged control arm can be seen in Figures 6 and 7.

The steering wheel is that component of the vehicle that connects the suspension system, the braking system and the steering system to the vehicle chassis, which is why the design and

production of the steering system wheel cannot be separated from the design and manufacture suspension system.



**Figure 6.** Forged control arm [5, 13]



**Figure 7.** Forged Auto Parts Control Arm for Trailers [14, 15]

Production of a steering knuckle (Figure 8) can be used in order to present some of the forming technologies, as well as machining processes. The first step in knuckle production is casting. It is important to select the type of casting technology, e.g. gravity, low pressure, high pressure, semi-solid, squeeze casting, etc. The quality and profitability of casting process depend on the metallurgical properties of the metal, mold design, process productivity, repeatability of the production conditions and properties of the part after heat treatment [6].



**Figure 8**. Casted and forged steering knuckle [7, 16, 17]

## *2.2 Machining of independent suspension elements*

Depending on the material that will be machined, characteristics including rigidity, spindle and attachment size, power and torque, and spindle velocity will be very important to define the most appropriate machine tool. Linear or rotating transfer machines or twin spindle machining centres are still preferred for high production volume, while machining centres (single or twin spindles) are preferred for lower production batches or mixed production batches. Achieving top quality and short cycle times of machining, along with minimising cost per piece have always been key goals for mechanical engineers for technology. The steering knuckle is usually produced in one or two set ups on machining centres [8].

Surfaces, parts and machining operations for typical front steering knuckles and typical rear knuckle are describes in Figure 9 [20]. Due to a limited number of position available in the tool magazine and the desire for short cycle times, the presented tools are be adapted to machining multiple operations. Due to a large variety of component concepts and shapes, the following pages describe most of the features concerning machining of a steering knuckle.



**Figure 9.** Surfaces operation machining [20]

1. Strut mount

2. ABS/ABR sensor location

3. Steering arm, tie rod location

4. lower ball joint location

5. Ball bearing location outer diameter machining

6. ball bearing location

7. Brake caliper fastening holes

8. wheel spindle

After the casting process, the portion of the knuckle which is used for connecting it to the damper and upper control arm is subjected to double side milling (Figure 10), using an indexable side cutter.

**Figure 10.** Double side milling [8]

This is followed by drilling a hole (Figure 11) for making a connection with the brake caliper.



**Figure 11.** Drilling [8]

Full side face milling of the lower control arms and tie rods is also necessary, as shown in Figure 12.



**Figure 12.** Full side face milling [8]

Drilling and chamfering of the edges of the joint used for connecting the steering knuckle with the lower control arm (Figure 13a) is the next step, followed by hole drilling for ABS/ABR sensor location (Figure 13b).



a)

b)

**Figure 13.** Drilling [8]

High precision boring (Figure 14) of the knuckle centre hole represents the next step.



**Figure 14.** High precision boring and sample tool for boring [8]

Following this, slotting is performed (Figure 15).



**Figure 15.** Slotting [8]

Figure 16 illustrates the final step, which includes face roughing and finishing.



**Figure 16.** Face roughing and finishing [8]

In the Figure 17 machining wheel spindle with special cutting tools is shown. Special tools are used for outside turning, chamfering, radius forming and longitudinal turning & chamfering.



**Figure 17.** Machining wheel spindle [20]

### 3.   CONCLUSIONS

There is a number of forming processes that are needed in order to produce intermediate forms of suspension components, and those are mainly forging and casting. After producing work pieces, machining of the same is performed. Machining processes that are used are drilling, milling, slotting, boring, as well as roughing and finishing of component's faces. It can be said that the same technologies are applied in case of independent and dependent suspension components. The leading dissimilarity is that independent suspension system integrates a much greater number of components, which are simultaneously more complex than dependent suspension components. This leads to a greater cost of production than in the case of dependent suspension. Be that as it may, cost is not the only factor which affects selection of the suspension type. Dependent suspension is more robust and provides better performance in case of extreme off-road applications, but the independent one contributes to

a greater vehicle ground clearance, reduction of mass, better fuel economy, as well as handling and ride comfort, so all of these factors have to be taken into account Many cutting tool manufacturers make recommendations for the choice of machining operations and tools. These recommendations are contained in this paper and should be kept in mind when designing the technology.

**REFERENCES**

[1]   Gadade B., Todkar R.G.: "Design, analysis of A-type front lower suspension arm in commercial vehicle", International Research Journal of Engineering and Technology Vol. 02, Issue 07, 2015, pp. 759-766.

[2]   Lajqi S., Pehan S., Lajqi N., Gjelaj A., Pšeničnik J., Emin S.: "Design of Independent Suspension Mechanism for a Terrain Vehicle with Four Wheels Drive and Four Wheels Steering", MOTSP 2012 Conference Proceedings, 2012, pp. 230-237.

[3]   Axle concept EasyTurn; Available from: https://www.zf.com/products/en/cars/products_45760.html, Accessed 29.10.2019.

[4]   Cole G.: "Automotive Chassis/Suspension Materials", Encyclopedia of Materials: Science and Technology, 2001, pp. 424-426.

[5]   European Aluminum Association, "Aluminum Automotive Manual", Brussels, 2011.

[6]   Sturm J., Schaefer W.: "Cast Iron – a predictable material: 25 Years of Modeling the Manufacture, Structures and Properties of Cast Iron", Materials Science Forum, Vol. 925, 2018, pp. 451-464.

[7]   Cast Iron And Cast Iron Steering Knuckle Castings, https://www.indiamart.com/proddetail/cast-iron-steering-knuckle-castings-19552380630.html, Accessed 26.01.2020.

[8]   Korloy, "Technical Information: Automotive industry", 2019.

[9]   Driven Solid Beam Axle, Available from: https://www.zf.com/products/en/cars/products_34560.html, Accessed 18.11.2019.

[10]  Solid Axle Industries D60 Kingpin Outer Knuckles (Ford), Available from: https://www.polyperformance.com/solid-axle-industries-d60-kingpin-outer-knuckles-ford-sa0760fkpk, Accessed 18.11.2019.

[11]  https://kmengineering.ru/bs/damping-elements-of-the-suspension-purpose-and-classification-of-car-suspension-brackets/ Accessed 05.12.2019.

[12]  http://www.ads-cz.com/independent_suspension_axles.html, Accessed 03.12.2019.

[13]  http://jxforgingparts.com/3-1-control-arm-forging.html, Accessed 05.12.2019.

[14]  https://thinkwell.en.made-in-china.com/product/leZJXRBPrSfC/China-Forged-Auto-Parts-Control-Arm-for-Trailers.html, Accessed 05.12.2019.

[15]  http://www.angstrom-usa.com/Upper-Control-Arms.html, Accessed 03.12.2019.

[16]  http://www.gohsyu.com/en/parts/chassis, Accessed 05.12.2019.

[17]  https://www.carid.com/motorcraft/front-driver-side-steering-knuckle-mpn-mef26.html, Accessed 08.12.2019.

[18]  Vlastimir D.: Nezavisno oslanjanje automobila, od projekta do dinamike vozila, Saobraćajni fakultet, Beograd, 1998.

[19]  https://www.sandvik.coromant.com/en-gb/industrysolutions/automotive/components/pages/knuckles.aspx, Accessed 03.12.2019.

[20]  Secotools, Technical information, Proven solutions for steering knuckle, Elenders, 2015.

*Intentionally blank*

# FUEL CELLS AND ELECTRIC VEHICLES

*Miroljub Adžić[1*]*

RESEARCH ARTICLE

**ABSTRACT:** The paper is concerned with fuel cell and hydrogen technologies and their application in electric vehicles. Beside positive energy balance effects, these technologies can decrease pollutants and carbon dioxide emissions. Fuel cells and hydrogen are quite mature technologies and already used in transportation systems. There are still drawbacks that prevent wider usage of fuel cell and hydrogen: current costs of electrical vehicles, fuel cells and hydrogen, hydrogen storage, very poor hydrogen infrastructure, lack of public awareness that hydrogen is a safe technology, already developed and applied battery technologies and political issues. Regarding the applicability in light vehicles, proton exchange membrane fuel cells together with hydrogen show good performance. It would not be a surprise that in the future hydrogen might affect the geo-strategy concepts based on fossil fuels.

**KEY WORDS**: fuel cells, electric vehicles, hydrogen

*[1]Miroljub Adžić, PhD prof., University of Belgrade Faculty of Mechanical Engineering, K. Marije 16, 11000 Beograd, mikce2001@gmail.com (\*Corresponding author)*

# GORIVE ĆELIJE I ELEKTRIČNA VOZILA

**REZIME**: Rad se bavi tehnologijama gorivih ćelija i vodonika i njihovom primenom u električnim vozilima. Pored pozitivnih efekata energetskog balansa, ove tehnologije mogu smanjiti zagađivače i emisiju ugljen-dioksida. Gorive ćelije i vodonik su prilično zrele tehnologije i već se koriste u transpotrnim sistemima. Još uvek postoje nedostaci koji sprečavaju veću upotrebu gorivih ćelija i vodonika: trenutni troškovi električnih vozila, gorivih ćelija i vodonika, skladištenje vodonika, veoma loša infrastruktura za snabdevanje vodonikom, nedostatak znanja javnog mnjenja da je vodonik sigurna tehnologija, već razvijena i primenjena tehnologija baterija i politička pitanja. Što se tiče primene u lakim vozilima, gorive ćelije sa proton-izmenjivom membranom zajedno sa vodonikom pokazuju dobre performanse. Ne bi bilo iznenađujuće da bi u budućnosti vodonik mogao uticati na koncepte geo-strategija zasnovanih na fosilnim gorivima.

**KLJUČNE REČI**: gorive ćelije, električna vozila, vodonik

# FUEL CELLS AND ELECTRIC VEHICLES

*Miroljub Adžić*

## 1. INTRODUCTION

The main conclusion of Fuel Cell Seminar in 1992, which was supported by US Department of Energy, Commission of European Communities and Japan Fuel Cell Development Center, was: „Fuel cells represent a technology which could potentially replace internal combustion engines in all areas of ground transportation in the 21st century"[1]. In the meantime, although never fully supported, fuel cells have reached maturity, side by side with internal combustion engines, when it comes to power performance and reliability. One should keep in mind that these two devices substantially differ: fuel cells deliver electric, while engines deliver mechanical power. It appears that the long waited good news for fuel cells happened in January 2017 at the World Economic Forum in Davos, when thirteen word leading energy, transport and industry companies have launched a global initiative by establishing Hydrogen Council Coalition with the ambition to "Accelerate their significant investment in the development and commercialization of the hydrogen and fuel cell sectors as part of the future energy mix with appropriate policies and supporting schemes." The Coalition founders are Air Liquide, Alstom, Anglo American, BMW GROUP, Daimler, ENGIE, Honda, Hyundai Motor, Kawasaki, Royal Dutch Shell, The Linde Group, Total and Toyota [2]. In one year, a number of other world leading companies joined the Council.

## 2. FUEL CELLS

Fuel cells are electrochemical devices that are capable of directly converting chemical energy of a fuel into electrical energy. Although the fuel cell principle was discovered almost 200 years ago and a practical device is relatively simple, there are still problems not easy to solve and a room to improve the performance. What are the differences between combustion of a fuel or its utilization in a fuel cell? A combustion is a process in which fuel and oxidant are brought into state of a complex mixture of radicals, atoms and molecules that react andrecombine to combustion products. During the combustion process chemical energy of fuel converts into heat and work. Combustion in real devices mainly happens in a turbulent flow regimes. If we speak about gaseous, premixed combustion, depending on the turbulence intensity and scales, combustion may proceed as a distinctive laminar, two dimensional, thin flame front, or as three dimensional processes [3]. Unlike to combustion, fuel and oxidant do not meet as such in fuel cells, Figure 1. They are physically separated by an <u>electrolyte</u>, a substance that <u>must be an insulator for electrons, good ion conductor and impermeable for gases</u>. Hydrogen, the basic fuel for fuel cells, is ionized to a proton and an electron: $H \rightarrow H^+ + e^-$. The proton is transported through electrolyte to react with oxygen, the electron is picked up by an electrode (anode) and transported into an electric circuit. By transporting ions and electrons electric current is generated and electric work is being done. The energy balance of the process is on the account of chemical energy of fuel which is converted into electrical work and to less extent into heat. There are different types of fuel cells, classified on different grounds, but it is mostly common to be classified by the type of electrolyte. However, the operating principle is similar for all types. For automotive use proton exchange membrane fuel cells (PEMFC) are the best suited. Keeping in mind the aim of this paper, only hydrogen and PEMFC are considered. This will not affect the general thermo and electrochemical analysis of fuel cell operation. A more detailed schematics of a proton exchange membrane fuel cell is shown in Figure 2. The PEMFC electrolyte is a sulfonated tetrafluoroethylene based fluoropolymer-copolymer, in the form of a thin plastic

membrane. Between the electrode and the electrolyte (membrane) there are two layers: a gas diffusion layer (GDL), which enables diffusion of gases and transport of electrons, and a catalyst layer, a carbon supported platinum catalyst where main reactions take place. The gaseous fuel (hydrogen) continuously flows over the anode while the oxidant (air) over to the cathode. The $H_2$ molecules pass through GDL and adsorb onto the catalyst layer where breaking of the H-H bond happens and atomic hydrogen adsorbs onto the surface. In the presence of $H_2O$ the adsorbed hydrogen desorbs as proton ($H^+$) while the liberated electron ($e^-$) is conducted to anode and further into the external electric circuit. The transport of protons $H^+$ has to overcome chemical and electrostatic field energy barriers, the sum of which is net energy barrier, as shown in Figure 3. Protons are transported through the electrolyte where at the cathode catalyst layer two protons react with oxygen and with two electrons coming via the closed external electric circle, doing electric work, producing only $H_2O$ and heat [4-6]. The overall reaction mechanism is complex, still not completely understood. The role of a platinum based catalyst is crucial. It substantially lowers the activation energies of reactions and accelerates the rate controlling steps.
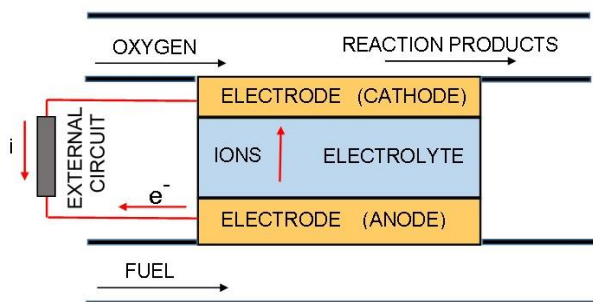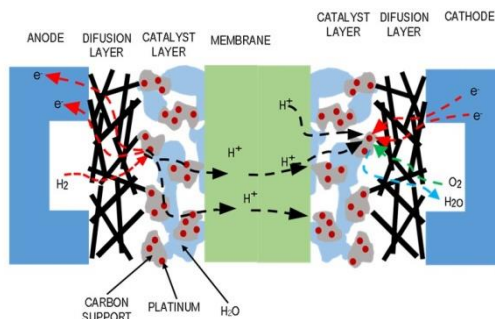


**Figure 1.** Schematic of fuel cell



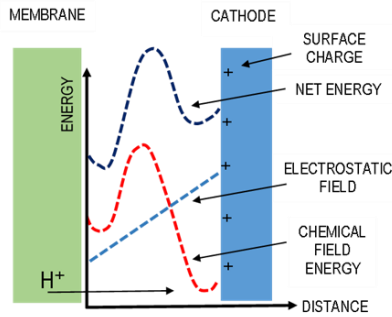**Figure 2.** Schematic of the fuel cell process

**Figure 3.** Schematic of fuel cell membrane-cathode energy field

Fuel cells can be fuelled by any fuel, but presence of carbon, sulphur and some other components can pose very serious problem depending on the fuel cell type. For that reason hydrogen is considered the ultimate fuel for fuel cells. One should notice that contrary to combustion, which is a three dimensional process, a fuel cell operates as a surface based process. This is one of the main reasons why combustion can deliver hundreds of megawatts of thermal power per unit volume of combustor while fuel cells are for orders of magnitude less effective.

### 2.1 Thermo and Electrochemistry of a Fuel Cell

We consider a fuel cell a reversible isothermal open thermodynamic system, with steady flow, negligible changes of potential and kinetic energy. By combining the first and the second law of thermodynamics we get

$$TdS = dU + pdV + \delta A = dH + \delta A, \text{ J/mol} \tag{1}$$

where T stands for absolute temperature, S entropy, U internal energy, V volume, A any other work except pdV and H enthalpy. From this equation follows that the maximum available work a system can deliver, $\delta A$, is

$$\delta A = TdS - dH \tag{2}$$

If we introduce the Gibbs free energy (available work) function $\Delta G$ term

$$dG = -\delta A = dH - TdS \tag{3}$$

and if only the electric forces do the work, then the work done by a system is

$$\Delta A = -\Delta G = Eit \tag{4}$$

where E is electric potential (voltage) delivered by a fuel cell, i is electric current flowing during period of time t. From (4) the electric potential E is

$$E = -\Delta G/it \tag{5}$$

The equation (5) shows that a fuel cell potential depends only on change of Gibbs energy, which is a unique characteristic of each fuel-oxidant system. In general, the potential is about 1 V.

Let us explain the operation of fuel cells fuelled by hydrogen. The overall chemical reaction is

$$H_2 + 1/2\ O_2 = H_2O \tag{6}$$

The process starts with ionization of a hydrogen molecule

$$H_2 = 2H^+ + 2e^- \tag{7}$$

One mol of hydrogen ($6.023\ 10^{23}$ molecules) is ionized to $2*6.023\ 10^{23} = 12.046\ 10^{23}$ protons and $12.046\ 10^{23}$ electrons. The charge of an electron is $1.602\ 10^{-19}$ C (coulombs), therefore the total charge q of free electrons is 192 970 C/mol. Keeping in mind that electric current is defined as a flow of electric charge q per time, i = q/t, we have

$$E = -\ \Delta G/it = -\ \Delta G/it = -\ \Delta G/q \tag{8}$$

As the change of Gibbs energy, $\Delta G$ for hydrogen-oxygen reaction (at T = 298 K, atmospheric pressure and water in liquid state) is – 237 245 J/mole, the electric potential of a fuel cell is

$$E = -\ \Delta G/q = 237\ 245/192\ 970 = 1.229, \ \ J/C\ or\ V$$

We should keep in mind that the value of calculated potential is theoretical one, at electrostatic conditions. Fuel cells appear to deliver electric energy in an elegant and efficient way. In practice a fuel cell faces a number of complex problems. With the onset of electric current the voltage decreases due to the onset of activation polarization (voltage losses by overcoming the activation energy needed to transport ions through the established electro-chemical field at the surfaces of electrodes), ohmic (Joule effect – heat generated by current flow) and mass transport losses (consumption of reactants induces concentration gradients which affect the fuel cell voltage as the supply of reactants is governed by Fick's law of molecular diffusion). Typical voltage and power curves of hydrogen fuelled PEMFC are shown in Figure 4 [7].
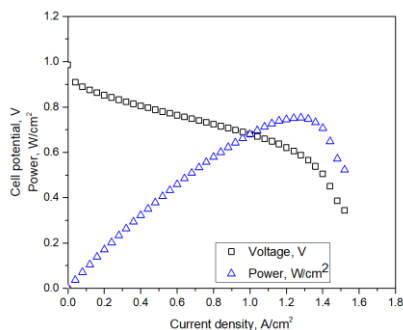


**Figure 4.** Typical voltage and power curves of an actual PEMFC fuel cell as a function of current density per geometrical unit area of membrane

The decrease of voltage with current are actually losses due to the kinetic effects of polarization activation (needs time to free the electrode surfaces from already occupied sites to take place for adsorption of new ions), ohmic (Joule loses Ri2) and mass transfer losses (Fick's law, *Ddc/dx*, decrease of concentration gradient).

The absolute (theoretical) efficiency of a fuel cell η is defined as the ratio between maximum available work $\Delta G$ and the heat of combustion $\Delta H$ of a fuel

$$\eta = \Delta G/\Delta H \qquad (9)$$

For hydrogen-oxygen and liquid $H_2O$, $\eta = 237\ 245/285\ 830 = 0.83$; for water in gaseous state, $\eta = 0.945$; for methane and liquid water, $\eta = 0.92$. As one can see the absolute efficiency depends only on fuel used, not on fuel cell type. In practice the efficiency is significantly lower. It is interesting to compare absolute (theoretical) efficiency of fuel cell hydrogen fuelled, and the Carnot cycle efficiency, Figure 5.
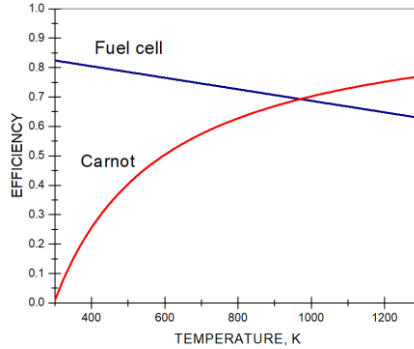


**Figure 5.** Comparison of fuel cell and Carnot cycle efficiency at lower temperature 298 K, [11]

Only at high temperatures over about 1000 K Carnot efficiency becomes superior to that of fuel cells. Keeping in mind that PEMFC operates at temperatures of about 100 K, its superiority over efficiency of Carnot is evident.

The electrical efficiency $\eta_e$ of a fuel cell is defined as the ratio of electrical power generated and the power of combustion based on the upper heating value of fuel used

$$\eta_e = Ei/\Delta H\dot{m} \qquad (10)$$

where $\Delta H$ is the higher heat of combustion of fuel and $\dot{m}$ is the fuel mass flow rate (kg/s). The electrical efficiency of fuel cell stacks can reach $0.55 - 0.60$ when hydrogen fueled.

As just shown, fuel cells are low voltage DC devices with the voltage output of about 1 Volt. For practical purposes, in order to increase the voltage and power, individual fuel cells are stacked in series, stacks, Fig. 6. A stack compared with unit cell is generally far more difficult to operate, because of more complicated mass, heat, liquid water and electric current management resulting in the decrease of efficiency, reliability and life of fuel cells.



**Figure 6.** Ballard fuel cell stack

The theoretical effects of temperature and pressure on fuel cell voltage can be deduced from eq. 8 where $E = -\Delta G/q$ and from $\delta (\Delta G)/\delta p = \Delta V$, where $\Delta V$ is the volume change of particular reaction. One should keep in mind that with the increase of temperature, $\Delta G$ increases (becomes less negative) but that affects the voltage of the order of millivolts, while the change of volume, e.g. for hydrogen fuel cell, is large, therefore the effect of pressure on voltage is evident. Nevertheless, in practice, these effects are much more complicated due to the effects of stack design, size, operating temperature and pressure, heat and mass transfer management and others.

It is worth noting that an electric battery is also an electrochemical electric energy source, but contrary to a fuel cell that can theoretically run for any period of time, as long as fuel and oxygen are supplied, a battery is just energy storage with limited capacity.

### 2.2 Fuel Cell Performance

The technology of PEMFCs is fully matured and in some elements better or in line with other systems like internal combustion engines and batteries. It is a question of performance, cost, primary energy sources, infrastructure and a policy to what extent PEMFC will be used in electric vehicles [7-14]. The brief visual comparison of some significant performance, based on the status in 2015/2017 are given in Figures 7-10 and Table 1. (The performance of fuel cells, motors and batteries, used in this paper, are the manufacturers' published data, as given). The efficiency of PEMFC (ratio between FC electric power and the chemical energy flow) including expectations in the future [5] and the last achievements in thermal efficiency of the Toyota gasoline engine is shown in Figure 7. The supremacy of fuel cell is impressive. Regarding mass to power ratio, life and startup time, Table 1 [5], as we can see, in next 10-15 years the mass to power ratio of PEMFC is planned to decrease three times, the life time to increase almost three times, and startup time to decrease for an order of magnitude. Even now the startup time is quite acceptable for transportation vehicles, two minutes. Comparison of mass to power ratio of PEMFC, internal combustion engine, electric drive and turboprop, as a function of power, is shown in Figures 8 and 9 [11].
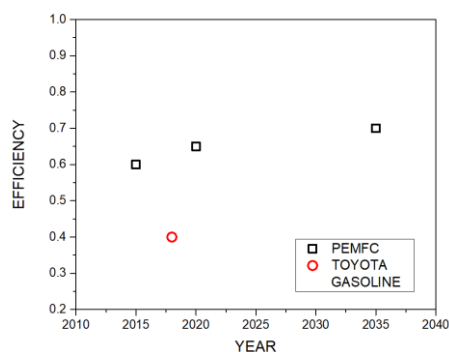


**Figure 7.** Efficiency of PEMFC and Toyota gasoline engine (2018)

**Table 1.** Performance indicators of PEMFC

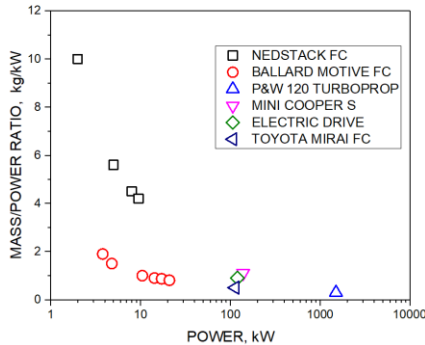| PEMFC fuel cell | Mass / Power ratio, kg/kW | Lifetime, h | Startup time, for a stack, seconds |
|---|---|---|---|
| Short term (5-10 years) | 0.5-0.2 | 20000 | 120 |
| Mid-term (10 to 15 years) | 0.25 – 0.17 | 40000 | 60 |
| Long term ( >>15 years) | < 0.15 | 50000 | 10 |



**Figure 8.** Mass to power ratio of PEMFCs (Nedstack, Ballard), internal combustion engine (Mini Cooper S-BMW), electric drive and turboprop engine (Pratt and Whitney 120)

As expected, the specific mass decreases with the power increase. It is worth noting that some of the Ballard fuel cells are at least as good as internal combustion engines and electro drives, but the recent efforts of Toyota resulted in very impressive results. Toyota managed the technological leap in a couple of years. The mass to power and volumetric power ratios of the Toyota PEMFC are the same as modern internal combustion engines and electric drives. In conclusion: the PEMFC mass-volume-power performance has reached the level of internal combustion engines and electric drives.
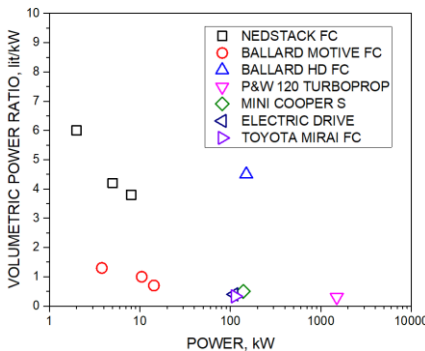


**Figure 9.** Volume to power ratio of PEMFC (Nedstack, Ballard), internal combustion engine (Mini Cooper S-BMW), electric drive and turbo-shaft engine (Pratt and Whitney 120)

The cost of PEMFC system primarily depends on number of units produced. Prediction of PEMFC cost in 2017 is given in Figure 10 [5]. It is interesting that the effect of year of production is rather small. It is expected that in 2025 the cost will be about 10% lower. At the moment the Toyota fuel stack cost is about $ 11,000 for annual production of 3,000 units. It is expected that with annual production of 30,000 the cost will drop to $ 8,000.
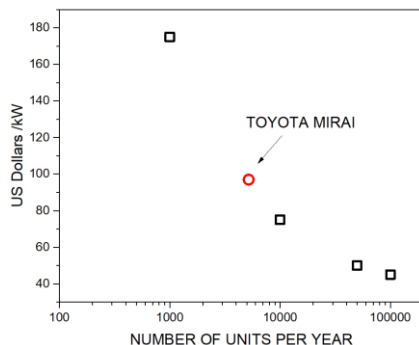


**Figure 10.** An 80 kW fuel cell power system for transportation prediction (2015), as a function of number of sold units

## 3.   HYDROGEN

A chemical energy source to run a fuel cell can be any fuel, but hydrogen is far the most appropriate. Some important properties of hydrogen are given in Table 2 [5].

**Table 2.** Properties of hydrogen

| Gaseous hydrogen | |
|---|---|
| Density (kg/m$^3$ at  273 K, 1.013 bar) | 0.089 |
| Lower heating value (MJ/kg) | 120.0 |
| Lower heating value (MJ/m$^3$) | 10.68 |
| Stoichiometric air fuel ratio (m$^3$/m$^3$) | 2.38 |
| Liquid hydrogen | |
| Density (kg/m$^3$at 1.013 bar and  boiling temp. 20.3 K) | 70.9 |
| Critical temperature (K) | 33 |

Although the main constituent of space, free hydrogen is scarce in our environment and has to be produced. About 96% of world hydrogen production is via fossil fuels, about 50% from natural gas, 30% from oil and 18% from coal, by different technologies. It should be stressed that the production of one kg of hydrogen from fossil fuels evolves about 11 kg of $CO_2$. New important technologies like the microorganisms and algae production of hydrogen from biomass with decentralized production from biomass become available. Most of hydrogen is used as raw material in fertilizer, chemical, oil, metal, food, pharmaceutical and glass industries. World consumption of hydrogen in 2016 was about 85 million tons, growing steadily. New developments are in the areas of innovative water electrolysers that can provide low price hydrogen production based on polymer-membrane

and solid oxide fuel cell technologies. The attractive idea to get *h*ydrogen from natural gas reforming and use in low temperature fuel cells like PEMFC has serious drawback: platinum based electrode catalysts can be poisoned by impurities, such as carbon monoxide, which is a natural constituent of the reformate. Besides, the very concept of fuel cells' low impact on the environment is jeopardized by high $CO_2$ emission when using hydrogen produced from fossil fuels. Hydrogen for fuel cells ought to be produced by lower impact systems, e.g., wind, solar or nuclear energy water electrolysis. At a glance, it does not look reasonable to produce electric energy by any method, use it to get hydrogen by water electrolysis and use it in a fuel cell to get electric energy again. The point is the energy accumulation effect of hydrogen storage that can help solving intermittency, fast fluctuations and surplus of wind and solar energies which can disrupt the electric grid balance and planning, as power plants cannot quickly adjust their production and balance total energy supply and demand. We have recently witnessed unimaginable situation when German producers of electric power paid some consumers to switch on and use electric utilities. And of course, the intentional production of hydrogen to be used in fuel cells and other purposes makes clear sense. One should also notice as well a very important fact that by this approach the total water balance in nature is zero. The main problems when using hydrogen in fuel cells or other energy production devices are low volumetric heat of combustion, rather poor storage properties, lack of infrastructure, cost, public stereotype that hydrogen is dangerous and lack of internationally homogenized standards and regulations.

Germany could be a good example of correlation between impressive increase of production of solar and wind based electric energy and the support of electric vehicles, hydrogen and fuel cells, Figure 11 [15]. The situation in Japan is even more positive towards use of hydrogen.
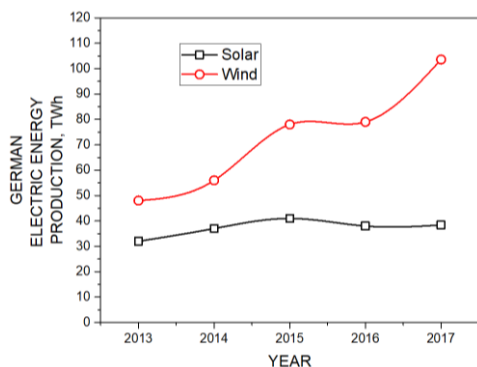


**Figure 11.** Wind and solar electric energy production in Germany during last five years

### 3.1 Hydrogen Storage

There is a number of hydrogen storage methods. From compressed gas cylinders, low temperature high pressure liquid, to adsorption over new exotic materials. For passenger vehicles the standard compressed hydrogen pressure is 70 MPa, while 35 MPa is for light and heavy trucks. There have been many efforts on hydrogen storage optimization, development of pressurized cylinders, valves, pressure regulators, pressure and temperature sensors and also high efficiency hydrogen compressors. Beside classical systems, the innovative approach uses electrochemical compressors with efficiency of 4kWh/kgH$_2$ at 70 MPa. Table 3 presents some new storage systems [5].

**Table 3.** New hydrogen storage systems

| Materials | Energy storage |
|---|---|
| Nanotubes physisorption (high pressure, low temperature) | 13.2 MJ/kg |
| Nanotubes | 6 MJ/l |
| Graphene chemisorption | 9.6 MJ/kg |
| Polymer matrix | 10.8 MJ/kg |
| Hollow $Li_{20}B_{60}$ cage | 9.6 MJ/kg |

The serious drawbacks of the new storage systems are as follows:

- Only laboratory proved
- Expensive
- High pressure, low temperature needed
- Low rates of sorption/desorption.

Hydrogen in a liquid state was abandoned, except for rocket propulsion, due to extreme conditions to fulfil very low temperature of 20 K and high pressure. The energy storage of hydrogen storage systems capacities by mass and volume are shown in Figure 12 [11].
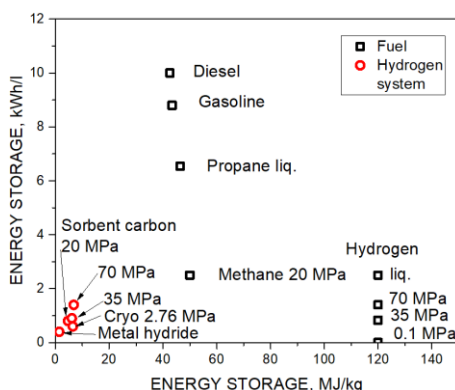


**Figure 12.** Energy storage capacities by mass and volume of fuels, hydrogen and hydrogen storage systems

It can be seen that the oil based fuels make good compromise between volumetric and mass energy storage, hydrogen has excellent mass but poor volumetric capacities. In general, hydrogen storage systems have low storage capacities either by mass or volume. About the hydrogen cost. Due to the political commitment and hydrogen technology production developments, the hydrogen price shows constant decrease and it is expected that in the next decade the price will be close to the price of liquid hydrocarbon fuels for transport, see Figure 13 [5]. The EU goal is the retail price at filing stations of 5.5 €/kg, or 0.046 €/MJ, thus approaching the 95 RON gasoline retail price in Germany of 1.49 €/l or 0.044 €/MJ, in September 2018. The retail price of hydrogen in August 2018 in Japan was 0.064 €/MJ.
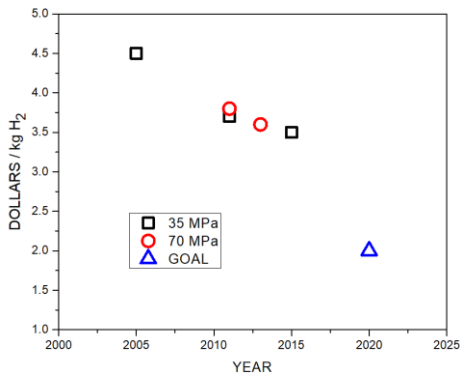
**Figure 13**. Centralized mass production of hydrogen, price prediction in USA for two standard storage pressures

The main obstacle for wider use of fuel cell vehicles is the lack of hydrogen infrastructure, number and distribution of hydrogen filling stations. In June 2018 there were less than 300 hydrogen filling stations worldwide [5]: 93 in Japan, 44 Germany, 39 USA, 12 South Korea, 11 England, 10 Denmark, 9 Norway, 9 in France and less than that in other countries. The good side is that hydrogen tank filling up is fast. It takes a couple of minutes.

## 4.  ELECTRIC BATTERIES

Electric batteries is proven and common energy storage technology. They are easy to use and operate. The drawbacks are low specific storage capaticies per mass and volume, price, and charging performance: either it takes hours or high power charging systems have to be used.  Besides,  fast charging induces  stresses and can lower the discharge capacity of a battery. At the moment two types of batteries are of main interest for electric vehicles: nickel-metal hydride (Ni-MH) and lithium-ion (Li-ion) batteries. The general performance indicators of electric batteries are presented in Table 4 [5]. As one can see, the mass to power ratio of batteries is planned to decrease three to six times, the lifetime is expected to reach over  1500 cycles in next 15 years.

**Table 4.** Performance indicators of batteries

| Batteries | Mass/energy stored ratio, kg/kWh | Gasoline kg/kWh | Hydrogen, kg/kWh Toyota Mirai, 700 bar cylinder | Lifetime, cycles |
|---|---|---|---|---|
| Short term (5-10 years) | 6-3 | | | > 1500 cycles; capacity drop < 30% |
| Mid-term (10 to 15 years) | 3–2 | 0.08 | 0.53 | |
| Long term ( >>15 years) | 2-1 | | | |

The capital cost for Li-ion battery pack per energy stored was about 400 US $/kWh, in 2015, with tendency to drop. In 2017 it was about 250 $/kWh. Further drop is expected to slow down with the expected cots in 2030 of about 100 $/kWh, Figure 14 [5].
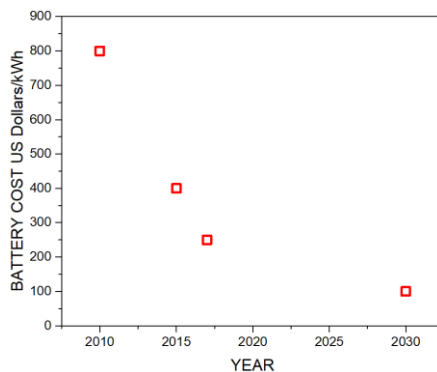
**Figure 14.** Electric battery cost

## 5. ELECTRIC VEHICLES

The concept of an electric vehicle is more than 200 years old. Electric vehicles have had ups and downs throughout the history. The first serious success in modern era, 20 years ago, comes from Toyota Prius hybrid electric vehicle equipped with nickel metal hydride battery. Later comes Tesla motors, and now there is practically no major car company without an electric vehicle in its production program. Regarding the propulsion systems, there is a steady progress in battery technology. The lithium-ion batteries have bloomed in last two decades. Electric motors and components have also been significantly improved. Also, the mass, volume, power, reliability, life of fuel cell.  The electric propulsion interest spreads also to air traffic, (major manufacturers Boeing and Airbus), marine, and transportation in general. The plug-in, plug-in hybrid, fuel cell vehicle technologies have been launched. Public electric vehicle chargers have been installed worldwide. The electric vehicle cost decreased and the environment has become much more supportive: free electric charging, free parking places, open yellow lanes, open access to otherwise forbidden areas in city centers and others. Although the drawbacks are serious, mass to storage ratio, low charging rates and cost, electric vehicles have become commercialized from all major and some specialized manufacturers.  The variety and combinations of propulsion systems, internal combustion engines, batteries, fuel cells, controls, fuels, fuel storage, drive components, energy management, materials, improvements and breakthroughs, costs and others is tremendous and very complex, making overall comparison of different types of vehicles difficult and questionable. Having that in mind and the aim of this paper to deliver a limited overview of fuel cell and hydrogen technologies and electric vehicles, this paper compares the cost of similar performance vehicles with different power systems manufactured by the same manufacturer, in this case Toyota, as an indicator of the technologies prospective, Figures 15-17 and Table 5.
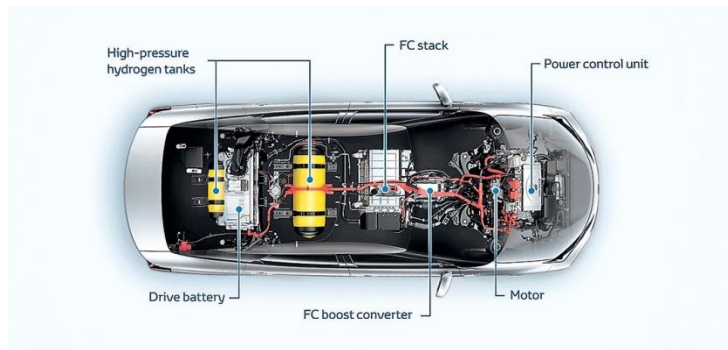
**Figure 15.** Toyota Mirai and hydrogen filling station



**Figure 16.** Toyota Mirai main components



**Figure 17.** Toyota Mirai powertrain

The Toyota Mirai is a midsize luxury 4 door sedan car. The powertrain consists of 113 kW, 335 Nm electric motor, PEMF fuel cell (370 cells) with maximum power output 114 kW, 0.50 kg/kW, 0.32 l/kW, two 70 Pa pressure hydrogen cylinders with total volume of 122.4 l and 84 kg mass, hydrogen storage of 4.8 kg or 160 kWh, 1.6 kWh nickel-metal hydride battery nominal voltage 244 V, capacity 6.5 Ah, the vehicle kerb weight is 1,850 kg, range about 500 km (planned to reach 1000 km in 2025!), max speed 178 km/h, acceleration 0-100 km/h in 9.6 seconds, refueling time 3-5 minutes. The battery assists fuel cell stack

during acceleration and stores recovered energy during deceleration. The Mirai fuel cell emission is water vapour, cost on the road $ 57,500.

**Table 5.** Cost of Toyota vehicles

| Type | Cost on the road $ |
|---|---|
| Avensis - (internal combustion engine; gasoline) | 30.200 |
| Prius Hybrid - (battery and internal combustion engine; gasoline) | 34.800 |
| Prius Plug-in Hybrid - (battery and internal combustion engine; gasoline) | 40.500[1] |
| Mirai  -  (fuel cell and battery; hydrogen) | 57.500[1] |

[1] Total sales of Prius plug-in hybrid was about 128,000 and 5,300 Mirai vehicles in 2017

Compared with the similar performance Toyota classical and electrical cars, Table 5, Mirai is expensive. With rise of production units, the cost is expected to decrease. An analysis shows that the cost of Mirai fuel cell of $ 11,000 could drop to $ 8,000 with increased production. Mirai is a hydrogen fuelled environment's best friend, which is an expensive position. Mirai is not a prestige car like Tesla S, a must for rich people, a matter of prestige, but a product of responsible national strategy policy, and vision of national future.

## 6.  CONCLUSIONS

- Fuel cells and hydrogen are matured technologies of equal performance (power, mass, volume, reliability, life) with internal combustion engines and electric drives, and already used for propulsion of vehicles.
- Fuel cells are superior to internal combustion engines regarding efficiency. When fuelled by hydrogen, fuel cells have excellent pollution and $CO_2$ emission performance.
- The main obstacles for wider usage are cost, hydrogen price and undeveloped hydrogen infrastructure.
- Breakthroughs in fuel cell and battery technologies are possible and expected which is not the case with hydrogen storage technologies.
- The cases of Germany and particularly Japan, show signs of accelerated and more aggressive utilization of hydrogen, meaning changes in strategy of national energy and geostrategic policies in the coming decades.
- Only time will tell what vehicle propulsion systems will prevail in the future.

## REFERENCES

[1]   The 1992 Fuel Cell Seminar, Tucson USA, 1992.
[2]   Hydrogen C.: Available from: http://hydrogencouncil.com/, Accessed 25.06.2018.
[3]   Mahjoub, M. A., Milivojević, A., Adžić, V., Živković, M., Fotev, V, Adžić, M.: "Numerical Analysis of Lean Premixed Combustor Fueled by Propane-Hydrogen Mixture", Thermal Science, Vol. 21, No. 6A, pp 2593-2602, 2017.
[4]   Fuel Cell Handbook, EG and G Technical Services, Morgantown, DOE, 2014.
[5]   US Dept. of Energy, Energy Efficiency and Renewable Energy, 2017.
[6]   Internationa Energy Agency, Hydrogen Production and Storage, OECD, Paris, 2006.
[7]   Adzic, M., Fotev,  V., Miivojevic, A., Adzic, V.: in the FP7,  "Efficient Use of Resources in Energy Converting Applications – PEMFC project", EURECA 2012-2015.

[8] Alaswad, A., Baroutaji, A., Achour, H., Carton, J.: "Developments in fuel cell technologies in the transport sector", International Journal of Hydrogen Energy, Vol. 41, Issue 37, 2016, pp 16499-16508.

[9] Pettersson, L., Westerholm, R.: "State of the art of multi-fuel reformers for fuel cell vehicles: problem identification and research needs", International Journal of Hydrogen Energy, Vol. 26, Issue 3, 2001, pp 243-264.

[10] Wang, Y, Dai, K., You, H., Gao, M.: "Research on the design of hydrogen supply system of 70 MPa hydrogen storage cylinder for vehicles", International Journal of Hydrogen Energy, Available online, September 2018.

[11] Adzic, M.: "Hydrogen and Fuel Cells for Aircraft Propulsion", Airbus Meeting, Munich, 2015.

[12] Alavi, F., Lee, E., de Wouw, N., de Schutter, B., Lukszo, Z.: "Fuel cell cars in a microgrid for synergies between hydrogen and electricity networks" Applied Energy Journal, Vol. 192, 2017, pp 296-304.

[13] Trade car view, Available from: https://www.tradecarview.com/specifications/toyota/, Accessed 25.06.2018.

[14] Simons, A., Bauer, C.: "The production and end-of-life processes for current and future proton exchange membrane fuel cell (PEMFC)", Applied Energy Journal, Vol. 157, 2015, pp 884-896.

[15] Eurostat,https://ec.europa.eu/Eurostat.

*Intentionally blank*

# INVESTIGATION OF DIESEL ENGINE OPERATED WITH DIESEL FUEL-BUTANOL BLENDS AND CETANE IMPROVER

*Hristo Stanchev[1*], Krasimir Markov[2]*

RESEARCH ARTICLE

**ABSTRACT:** Experimental investigation of a common rail direct injection diesel engine is carried out, when working with diesel fuel in blends with 10% (B10), 15% (B15) and 20% (B20) *n*- butanol at different loads and speeds. The cetane number of the blends is lower than basic fuel and is corrected to these of the neat diesel fuel. The differences in brake specific fuel consumption (BSFC) and exhaust emissions are compared with the baseline operations (when working with the neat diesel fuel). The cetane improver 2-EthylHexil Nitrate is used. Six types of fuels are investigated: B10 and B10 with cetane improver, B15 and B15 with cetane improver, B20 and B20 with cetane improver. This approach shows that the BSFC for fuel blends with corrected cetane number is closer to this with neat diesel fuel, especially at higher engine speeds. The exhaust smoke (D) for blends with corrected cetane number is lower than the neat diesel fuel and blends without cetane improver. There is no clear trend for NOx emission.

---

[1]*Hristo Stanchev, PhD prof., University of Ruse, 8 Studentska St, 7017 Ruse, Bulgaria, hstanchev@uni-ruse.bg (*Corresponding author)*
[2]*Krasimir Markov, Assist. prof., University of Ruse, 8 Studentska St, 7017 Ruse, Bulgaria, krmarkov@uni-ruse.bg*

# ISTRAŽIVANJE DIZEL MOTORA KOJI RADI SA MEŠAVINOM DIZEL-BUTANOL GORIVA SA CETANSKIM POBOLJŠANJEM

**REZIME**: Eksperimentalno istraživanje dizel motora se Common rail direktnim ubrizgavanjem je realizovano korišćenjem mešavine dizel goriva sa: 10% (B10), 15% (B15) i 20% (B20) n-butanola pri različitim opterećenjima i brzinama. Cetanski broj mešavina je niži od baznog goriva i korigovan je na vrednosti za čisto dizel gorivo. Razlike u potrošnji goriva kočnice (BSFC) i emisije izduvnih gasova upoređene su sa osnovnim operacijama (kada se radi sa čistim dizel gorivom). Korišćen je 2-EthylHexil Nitrat za poboljšanje cetanskog broja. Ispitivano je 6 vrsta goriva: B10 i B10 sa cetanskim poboljšivaačem B15 i B15 sa cetanskim poboljšivačem, B20 i B20 sa cetanskim poboljšivačem. Ovaj pristup pokazuje da je BSFC za mešavine goriva sa korigovanim cetanskim brojem bliži onom sa čistim dizel gorivom, posebno na većim brzinama rada motora. Izduvni dim (D) za mešavine sa korigovanim cetanskim brojem je manji nego kod čistog dizel goriva i mešavina se bez cetanskog poboljšanja. Ne postoji jasan trend emisije NOx.

**KLJUČNE REČI**: dizel motor, n-butanol, mešavine goriva, cetanski broj, cetanski poboljšivače, emisija

# INVESTIGATION OF DIESEL ENGINE OPERATED WITH DIESEL FUEL-BUTANOL BLENDS AND CETANE IMPROVER

*Hristo Stanchev, Krasimir Markov*

## 1.  INTRODUCTION

The high emission standards for greenhouse gases exist using of different type of high alcohols as an alternative fuels (blends with standard fuel). The new low cost technology for butanol production and its very close characteristics to fossil fuels lead to active scientific work all around the world for replacement of part of these fuels with butanol. There are lot hurdles to be overtaken to use high percentage of butanol in blends with diesel fuel. Butanol has lower cetane number which resulted in different type of combustion process. The main advantage of butanol as a fuel for internal combustion engines are higher flash point (safer for distribution and storage), less corrosive influence on fuel system, less evaporative emission, lower emission of smoke, CO and HC due to high oxygen content and higher laminar flame speed resulted in enhance reactions. There is no clear tendency in NOx emission changes because of concurrent between lower temperature and higher oxygen content, but NOx emission can be effectively reduced due to high EGR rate without increasing in smoke emission [1, 3, 5, 6]. Using butanol as a fuel for diesel engines leads to extended ignition delay period and this increases heat release quantity. As a result the specific effective fuel consumption increases with higher percentage of butanol. The temperature of exhaust gases is lower and effective efficiency is higher [2, 4].

## 2.  EXPERIMENTAL RESULTS

### 2.1  Test rig description

An engine Fiat 1.9 JTD has been tested in laboratory condition on DC dynamometer. The fuel consumption is determined by mas flow method. For evaluation of emission components a 5-components gas analyser Auto Logic is used. For more precise NOx concentration measurement special analyser ECM NOx 5210 (g) is used. The exhaust smoke is measured by OPA-101 Nextech diesel smoke opacity meter. The technical specifications of equipment are given in next tables.

**Table 1.** Auto Logic 5-components gas analyzer

| Component | Range | Accuracy (rezolution) |
|---|---|---|
| HC | 0-2000 ppm | 1 ppm |
| CO | 0-15% | 0.001 vol.% |
| CO2 | 0-20% | 0.01 vol.% |
| O2 | 0-25% | 0.01 vol.% |
| NOx | 0-5000 ppm | 1 ppm |
| A/F ratio | 0-72 | 0.01 |

**Table 2.** ECM NOx 5210(g) analyzer

| Component | Range |
|-----------|-------|
| NOx | 0-8000 ppm |
| λ | 0.4 - 25 |
| AFR | 6.0 - 364 |
| Φ | 0.04 – 2.5 |
| $O_2$ | 0.0 – 25 Vol.% |
| FAR x 10 000 | 27 - 1667 |

The data from ECM gas analyzer are compensated depend on the pressure in place of NOx /O2 sensor

**Table 3**. OPA – 101 smoke opacity meter

| Parameter | Range (accuracy) |
|-----------|------------------|
| Opacity | 0,0 – 100% (0,01%) |
| Absorbtion coefficient K | 0,00– 21,42 m-1 (0,01 m-1) |
| Engine oil temperature | 0 – 120 $^o$C |
| Engine speed | 0 – 5000 min$^{-1}$ |

Experimental study has been carried out to investigate the impact of the different butanol-diesel blends on the engine performance and emission levels under a variety of operating conditions (load and speed). The cetane number of fuel mixture is corrected to these of neat diesel fuel – 51 points. For evaluation of influence of the lower cetane number of butanol-diesel blends on engine performance were conducted experiments with different fuel blends without cetane number corrections first. In references there is not exact cetane number of n-butanol. The data are as between 17 and 26 points. The cetane number of the butanol has been assumed 25 points in our case. This cetane number is used for calculation of quantity of cetane improver to be added to different fuel blends. Cetane improver 2-EthylHexil Nitrate, produced by "Very One" company is used. According to the technical specification of this product 100 ppm volume concentration increases cetane number with 0,28 points or 400 ppm approximately for 1 point increasing. Taking this into account, for the three fuel blend with 10, 15 and 20% butanol, the quantity of cetane improver for a liter fuel is given in Table 4.

**Table 4.** Quantity of cetane improver for reaching of fuel blends cetane number 51 points

| % butanol | Cetane number (CN) of the blend | Difference to 51 points | Quantity 2-Ethylhexil Nitrate, ml |
|-----------|----------------------------------|--------------------------|-----------------------------------|
| 10 | 48.4 | 2.6 | 1.04 |
| 15 | 47.1 | 3.9 | 1.56 |
| 20 | 45.8 | 5.2 | 2.08 |

The results from investigation are shown in graphical form. For comparison at every figure for certain concentration of butanol are shown the results, obtained for neat diesel fuel, the diesel-butanol blend and the diesel-butanol-cetane improver blend.

### 2.2 Analysis of the results

At engine speeds 1500 min$^{-1}$ and 2000 min$^{-1}$ cetane number of fuel does not have significant influence on the combustion process and consequently on the power and brake specific fuel

consumption (BSFC) for all types of blends. It is observed increase in NOx emissions and decrease in smoke emissions. At engine speed 2500 min$^{-1}$ (Figure 1 – 3) the correction of fuel blends cetane number has visible effect on the BSFC in comparison with the operation of the engine with fuel blends without cetane number correction. It is visible from the results that the BSFC does not differ from the engine operation with neat diesel fuel.
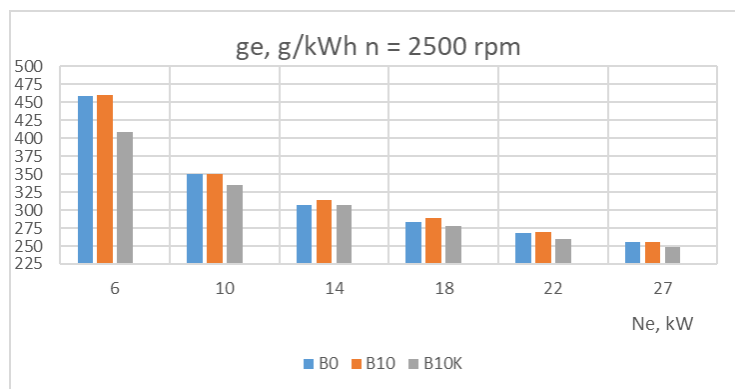


**Figure 1.** Change of BSFC (ge) at neat diesel fuel (B0), addition of 10% butanol (B10) and B10 with cetane improver (B10K)
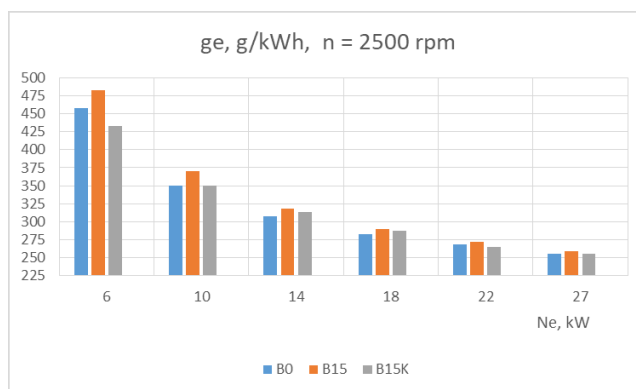


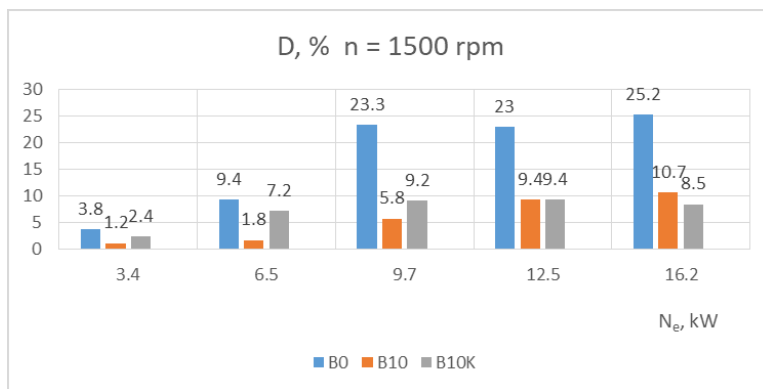**Figure 2.** Change of BSFC at neat diesel fuel (B0), addition of 15% butanol (B15) and B15 with cetane improver (B15K)

From the obtained result it can be concluded that with addition up to 20% butanol to diesel fuel is possible to keep engine performance the same as with neat diesel fuel, without any modifications in exist injection program. Any modification requires reprogramming of electronic control unit on the base of experimental defined optimal injection program (pilot injection quantity and timing, main injection timing and late injection timing) at operation with dieselbutanol blends.

As is mentioned above, addition of butanol to diesel fuel has contradiction influence over the NOx emissions. Lower cetane number of diesel-butanol blends leads to extended ignition delay and increased in-cylinder temperature and accordingly higher NOx emissions. Higher content of oxygen in butanol has the same influence. Conversely, higher boiling point of butanol reduces the flame temperature in the combustion chamber, which leads to

decrease in NOx emission. This effect is more crearly visible at low engine loads when the heat for evaporation exceeds the combustion temperature. Also, the presence of 2-ethylhexyl nitrate cetane improver introduces a new fuel-borne NOx formation mechanism to the combustion process, which increases NOx emissions. The increase in NOx emission is formed by the decomposition of the cetan improver. Reduction of smoke emissions, when using diesel-butanol blends, is due to increased content of oxygen in fuel blends.
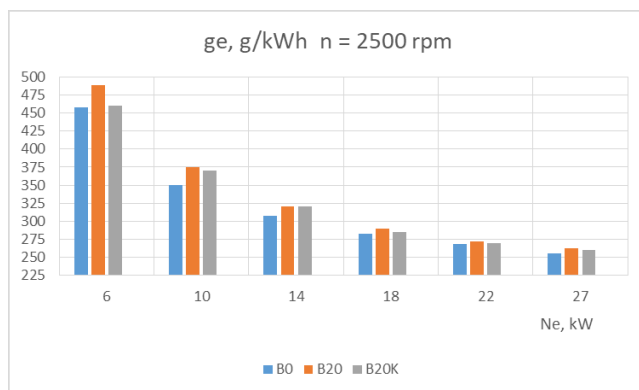


**Figure 3.** Change of BSFC at neat diesel fuel (B0), addition of 20% butanol (B20) and B20 with cetane improver (B20K)

Results for smoke (D) emissions at all investigated working regimes and fuel blends are shown in Figure 4 to Figure 12. There is not clear trend at different operation conditions. The main reason for this is different influence of ignition delay period at different engine speeds with correction of blend's cetane number. At higher loads, when cetane improver is added, the smoke emission is close to that without cetane improver. This effect reduces with increasing of butanol percentage in blends. For full estimation of the effect of fuel cetane number on the combustion process must be proceed in-cylinder pressure measurement (indicator diagram).



**Figure 4.** Change of smoke (D) at neat diesel fuel (B0), addition of 10% butanol (B10) and B10 with cetane improver (B10K)
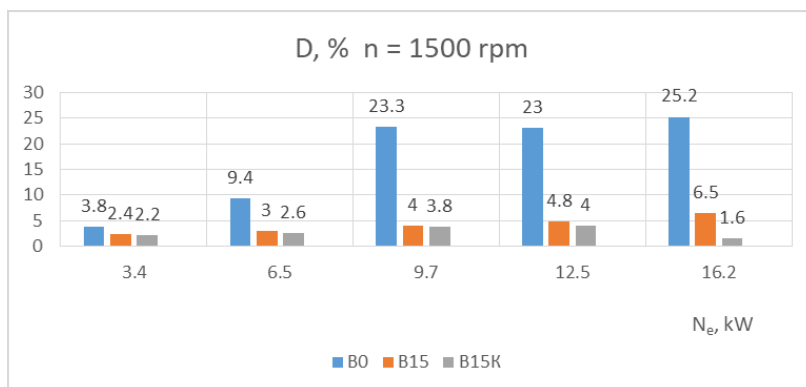
**Figure 5**. Change of smoke (D) at neat diesel fuel (B0), addition of 15% butanol (B15) and B15 with cetane improver (B15K)
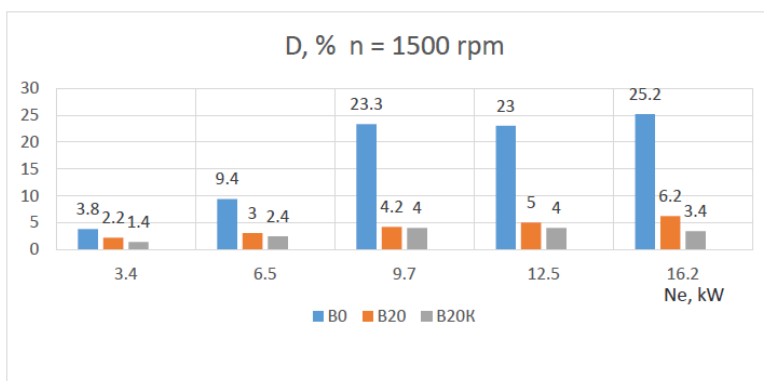


**Figure 6.** Change of smoke (D) at neat diesel fuel (B0), addition of 20% butanol (B20) and B20 with cetane improver (B20K)
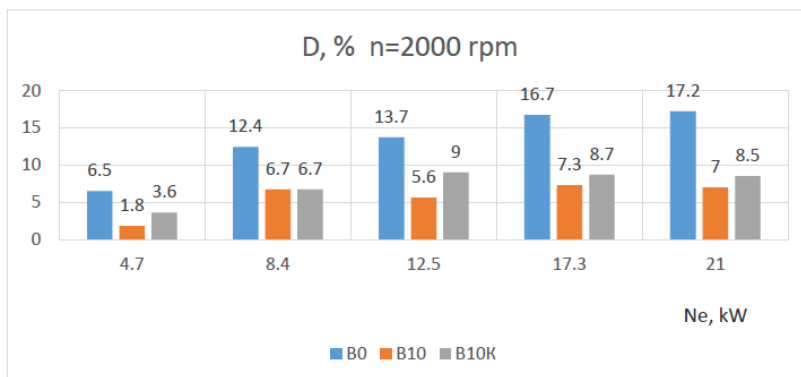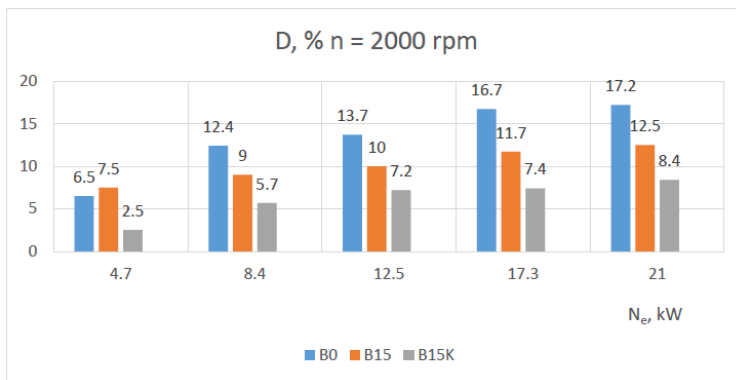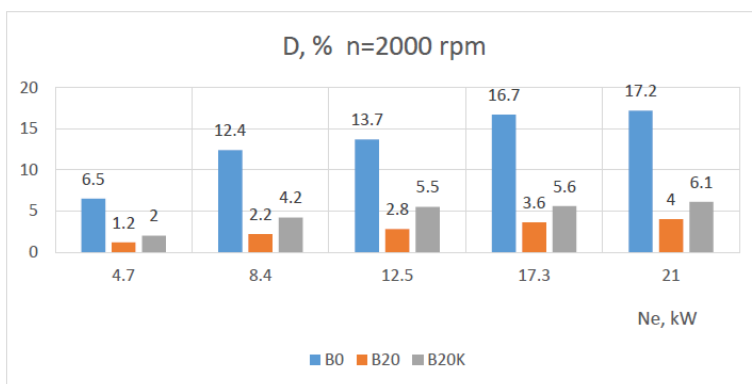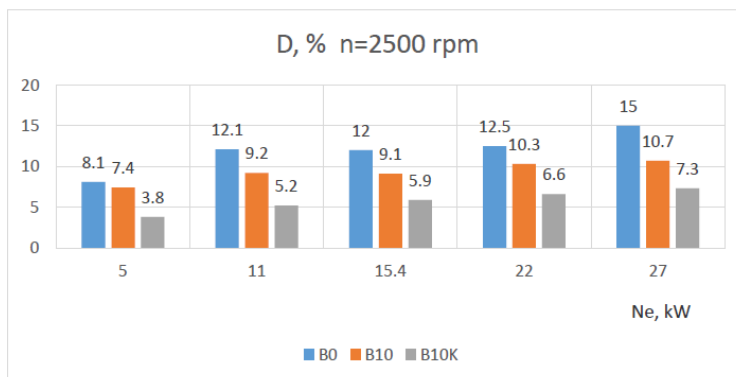


**Figure 7.** Change of smoke (D) at neat diesel fuel (B0), addition of 10% butanol (B10) and B10 with cetane improver (B10K)

**Figure 8.** Change of smoke (D) at neat diesel fuel (B0), addition of 15% butanol (B15) and B15 with cetane improver (B15K)



**Figure 9.** Change of smoke (D) at neat diesel fuel (B0), addition of 20% butanol (B20) and B20 with cetane improver (B20K)



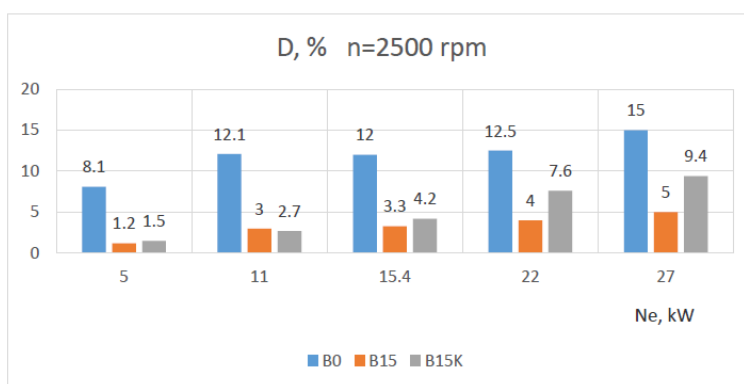**Figure 10.** Change of smoke (D) at neat diesel fuel (B0), addition of 10% butanol (B10) and B10 with cetane improver (B10K)

**Figure 11.** Change of smoke (D) at neat diesel fuel (B0), addition of 15% butanol (B15) and
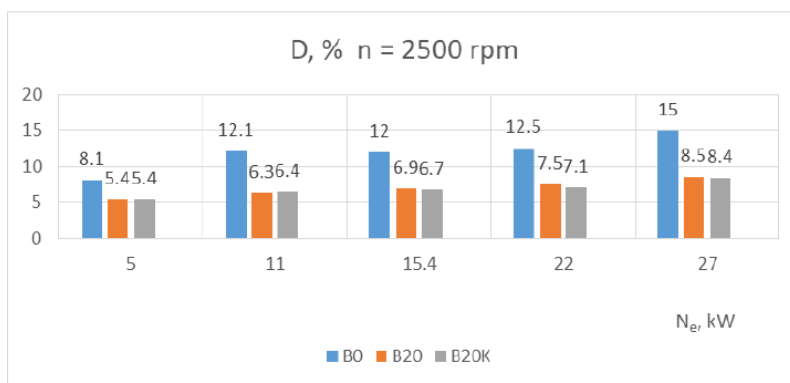B15 with cetane improver (B15K)



**Figure 12.** Change of smoke (D) at neat diesel fuel (B0), addition of 20% butanol (B20) and
B20 with cetane improver (B20K)

As an example, results for NOx emissions at engine speed n=2500 min$^{-1}$ and for all fuel
blends are shown in Figure 13 to Figure 15. It is evident, that there is not clear trend in NOx
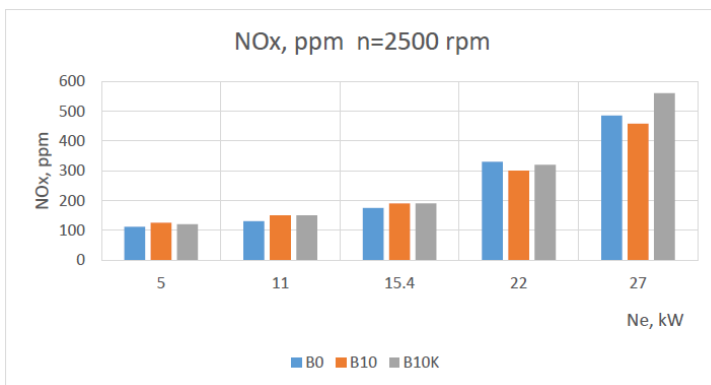concentration at different load conditions and fuel blends.

**Figure 13.** Change of NOx concentration at neat diesel fuel (B0), addition of 10% butanol (B10) and B10 with cetane improver (B10K)
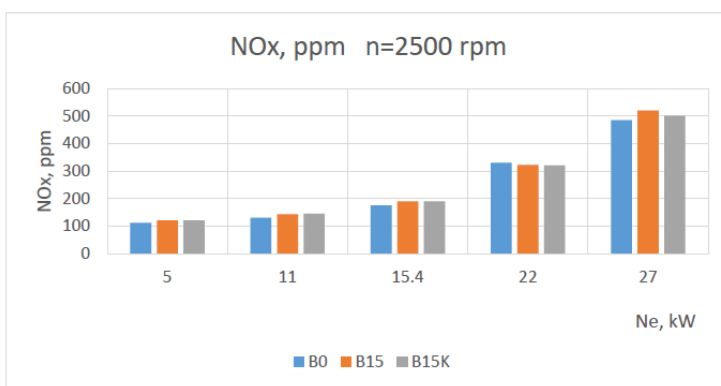


**Figure 14.** Change of NOx concentration at neat diesel fuel (B0), addition of 15% butanol (B15) and B15 with cetane improver (B15K)
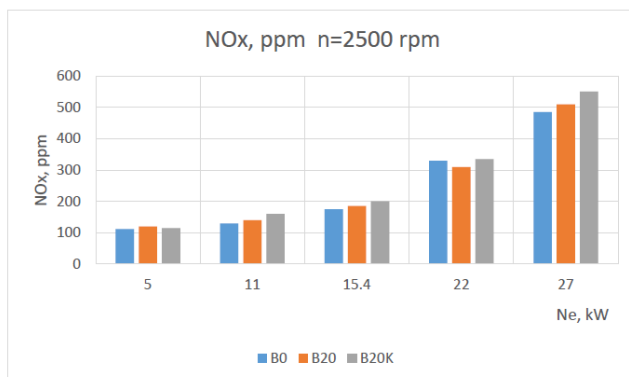


**Figure 15.** Change of NOx concentration at neat diesel fuel (B0), addition of 20% butanol (B20) and B20 with cetane improver (B20K)

## 3.  CONCLUSIONS

1.  Brake specific fuel consumption, when engine work with addition of cetane improver is almost equal to this with neat diesel fuel. The effect is better at higher engine speed due to stronger influence of fuel cetane number on the combustion process at these speeds.

2.  It is evident from experiment that fuel (fuel blends) cetane number has different influence on smoke emission at different engine speed. It is observed saving or slightly more or less smoke emissions, compare with engine operation without cetane improver.

3.  There is no need of engine control unit reprogramming when up to 20% n-butanol is added to diesel fuel and fuel blends cetane number is corrected.

## REFERENCES

[1]    Algayyim, S., Wandel, A., Yusaf, T., Hamawand, I.: "The impact of n-butanol and iso-butanol as components of butanol-acetone (BA) mixture-diesel blend on spray, combustion characteristics, engine performance and emission in direct injection diesel engine", Energy, Vol. 140, Part 1, 2017, pp 1074-1086.

[2]    Chen, Z., Liu, J., Han, Z., Du, B., Liu, Y., Lee, C.: "Study on performance and emissions of a passenger-car diesel engine fueled with butanol-diesel blends", Energy, Vol. 55, 2013, pp 638-646.

[3]    Dobre, A., Pană, C., Nuţu, N., Cernat, Al.; Bondoc, I. D.: "Bio-butanol-alternative fuel for Diesel engine" INMATEH-Agricultural Engineering, Vol. 42, Issue 1, 2014, pp 145-152.

[4]    Giakoumis, G.**,** Rakopoulos, C., Dimaratos, A., Rakopoulos, D.: "Exhaust emissions with ethanol or n-butanol diesel fuel blends during transient operation", Renewable and Sustainable Energy Reviews, Vol. 17, 2013, pp 170-190.

[5]    Karabektas, M., Hosoz, M.: "Performance and emission characteristics of a diesel engine using isobutanol–diesel fuel blends", Renewable Energy, Vol. 34, Issue 6, 2009, pp 1554-1559.

[6]    Rajesh Kumar, B., Saravanan S., Rana D., Nagendran A.: "A comparative analysis on combustion and emissions of some next generation higher-alcohol/diesel blends in a direct-injection diesel engine", Energy Conversion and Management, Vol. 119, 2016, pp 246-256.

**NOTIFICATION TO AUTHORS**

The Journal MVM publishes original papers which have not been previously published in other journals. This is responsibility of the author. The authors agree that the copyright for their article is transferred to the publisher when the article is accepted for publication.

The language of the Journal is English.

Journal *Mobility & Vehicles Mechanics* is at the SSCI list.

All submitted manuscripts will be reviewed. Entire correspondence will be performed with the first-named author.

Authors will be notified of acceptance of their manuscripts, if their manuscripts are adopted.

*INSTRUCTIONS TO AUTHORS AS REGARDS THE TECHNICAL ARRANGEMENTS OF MANUSCRIPTS*:

**Abstract** is a separate Word document, "*First author family name_ABSTRACT.doc*". Native authors should write the abstract in both languages (Serbian and English). The abstracts of foreign authors will be translated in Serbian.

This document should include the following: 1) author's name, affiliation and title, the first named author's address and e-mail – for correspondence, 2) working title of the paper, 3) abstract containing no more then 100 words, 4) abstract containing no more than 5 key words.

**The manuscript** is the separate file, „*First author family name_Paper.doc*" which includes appendices and figures involved within the text. At the end of the paper, a reference list and eventual acknowledgements should be given. References to published literature should be quoted in the text brackets and grouped together at the end of the paper in numerical order.

Paper size: Max 16 pages of B5 format, excluding abstract
Text processor: Microsoft Word
Margins: left/right: mirror margin, inside: 2.5 cm, outside: 2 cm, top: 2.5 cm, bottom: 2 cm
Font: Times New Roman, 10 pt
Paper title: Uppercase, bold, 11 pt
Chapter title: Uppercase, bold, 10 pt
Subchapter title: Lowercase, bold, 10 pt
Table and chart width: max 125 mm
Figure and table title: Figure _ (Table _): Times New Roman, italic 10 pt

Manuscript submission: application should be sent to the following e-mail:

**mvm@kg.ac.rs ; lukicj@kg.ac.rs**
or posted to address of the Journal:
**University of Kragujevac – Faculty of Engineering**
**International Journal M V M**
**Sestre Janjić 6, 34000 Kragujevac, Serbia**

The Journal editorial board will send to the first-named author a copy of the Journal offprint.

## OBAVEŠTENJE AUTORIMA

Časopis MVM objavljuje orginalne radove koji nisu prethodno objavljivani u drugim časopisima, što je odgovornost autora. Za rad koji je prihvaćen za štampu, prava umnožavanja pripadaju izdavaču.

Časopis se izdaje na engleskom jeziku.

Časopis *Mobility & Vehicles Mechanics* se nalazi na SSCI listi.

Svi prispeli radovi se recenziraju. Sva komunikacija se obavlja sa prvim autorom.

## *UPUTSTVO AUTORIMA ZA TEHNIČKU PRIPREMU RADOVA*

**Rezime** je poseban Word dokument, "*First author family name_ABSTRACT.doc*". Za domaće autore je dvojezičan (srpski i engleski). Inostranim autorima rezime se prevodi na srpski jezik. Ovaj dokument treba da sadrži: 1) ime autora, zanimanje i zvanje, adresu prvog autora preko koje se obavlja sva potrebna korespondencija; 2) naslov rada; 3) kratak sažetak, do 100 reči, 4) do 5 ključnih reči.

**Rad** je poseban fajl, „*First author family name_Paper.doc*" koji sadrži priloge i slike uključene u tekst. Na kraju rada nalazi se spisak literature i eventualno zahvalnost. Numeraciju korišćenih referenci treba navesti u srednjim zagradama i grupisati ih na kraju rada po rastućem redosledu.

Dužina rada: Najviše 16 stranica B5 formata, ne uključujući rezime
Tekst procesor: Microsoft Word
Margine: levo/desno: mirror margine; unurašnja: 2.5 cm; spoljna: 2 cm, gore: 2.5 cm, dole: 2 cm
Font: Times New Roman, 10 pt
Naslov rada: Velika slova, bold, 11 pt
Naslov poglavlja: Velika slova, bold, 10 pt
Naslov potpoglavlja: Mala slova, bold, 10 pt
Širina tabela,dijagrama: max 125 mm
Nazivi slika, tabela: Figure __ (Table _): Times New Roman, italic 10 pt

Dostavljanje rada elektronski na E-mail: **mvm@kg.ac.rs ; lukicj@kg.ac.rs**

ili poštom na adresu Časopisa
**Redakcija časopisa M V M**
**Fakultet inženjerskih nauka**
**Sestre Janjić 6, 34000 Kragujevac, Srbija**

Po objavljivanju rada, Redakcija časopisa šalje prvom autoru jedan primerak časopisa.